RESEARCH ARTICLE

Key Points:
- We presented an upscaling scheme for including erosion-induced lateral soil and carbon transfers into a global land surface model
- Our model is a useful tool to estimate the impacts of climate and land cover changes on erosion-induced soil carbon loss at large scale
- Model application for the Rhine basin demonstrates that erosion-induced soil carbon losses substantially reduce soil carbon stocks

Supporting Information:
- Supporting Information S1

Correspondence to:
H. Zhang,
sysuzhaicheng@163.com

Simulating Erosion-Induced Soil and Carbon Delivery From Uplands to Rivers in a Global Land Surface Model

Haicheng Zhang[1,2] (iD), Ronny Lauerwald[1,2] (iD), Pierre Regnier[1], Philippe Ciais[2], Wenping Yuan[3] (iD), Victoria Naipal[2,4], Bertrand Guenet[2] (iD), Kristof Van Oost[5], and Marta Camino-Serrano[6]

[1]Department Geoscience, Environment and Society, Université Libre de Bruxelles, Brussels, Belgium, [2]Laboratoire des Sciences du Climat et de l'Environnement, IPSL-LSCE CEA/CNRS/UVSQ, Gif sur Yvette, France, [3]School of Atmospheric Science, Sun Yat-sen University, Guangzhou, China, [4]Department of Geosciences, École Normale Supérieure, Paris, France, [5]UCLouvain, TECLIM - Georges Lemaître Centre for Earth and Climate Research, Louvain-la-Neuve, Belgium, [6]CREAF, Cerdanyola del Vallès, Spain

Abstract Global water erosion strongly affects the terrestrial carbon balance. However, this process is currently ignored by most global land surface models (LSMs) that are used to project the responses of terrestrial carbon storage to climate and land use changes. One of the main obstacles to implement erosion processes in LSMs is the high spatial resolution needed to accurately represent the effect of topography on soil erosion and sediment delivery to rivers. In this study, we present an upscaling scheme for including erosion-induced lateral soil organic carbon (SOC) movements into the ORCHIDEE LSM. This upscaling scheme integrates information from high-resolution (3″) topographic and soil erodibility data into a LSM forcing file at 0.5° spatial resolution. Evaluation of our model for the Rhine catchment indicates that it reproduces well the observed spatial and temporal (both seasonal and interannual) variations in river runoff and the sediment delivery from uplands to the river network. Although the average annual lateral SOC flux from uplands to the Rhine River network only amounts to 0.5% of the annual net primary production and 0.01% of the total SOC stock in the whole catchment, SOC loss caused by soil erosion over a long period (e.g., thousands of years) has the potential to cause a 12% reduction in the simulated equilibrium SOC stocks. Overall, this study presents a promising approach for including the erosion-induced lateral carbon flux from the land to aquatic systems into LSMs and highlights the important role of erosion processes in the terrestrial carbon balance.

Plain Language Summary Global land surface models (LSMs) are the main tools used to simulate the terrestrial carbon (C) cycle and to predict its response to climate and land cover changes. Currently, the processes of vertical C fluxes between soils, plants, and the atmosphere (e.g., photosynthesis, plant growth, and litter and soil organic matter decomposition) has been well represented in many LSMs; however, the lateral soil C delivery through the river network caused by water erosion is still missing in most LSMs. This study introduces a LSM approach which is suitable to simulate the large-scale soil C delivery from upland soils to inland waters at high temporal resolution (daily) and accounting for the small-scale (~90 m) spatial variability in topography and soil properties. Evaluation of our model in the Rhine catchment demonstrates a good performance with regard to reproducing the spatial and temporal (daily, seasonal, and interannual) variability of soil C delivery rate from uplands to river networks at large spatial scale and for exploring the impacts of changes in vegetation cover (land use change) and climate (e.g., changes in rainfall amounts and regimes) on the regional soil C balance.

1. Introduction

The lateral carbon (C) transfer from land to ocean through water erosion and inland waters transport processes plays an important role in the regional to global terrestrial C balance on time scales ranging from decadal to millennial (Ciais et al., 2008; Regnier et al., 2013; Galy et al., 2015). The magnitude of this lateral C flux is, however, highly uncertain. For instance, the study of Cole et al. (2007) estimated a global C delivery from land to inland waters of 1.9 Pg C yr^{-1} (1 Pg = 10^{15} g), while the study of Drake et al. (2018) estimated

that this flux could reach up to 5.1 Pg C yr^{-1} globally. A significant proportion of this flux is due to erosion of soil organic C (SOC) delivered to rivers as particulate organic C. Along with the lateral translocation of SOC, the terrestrial-atmosphere C exchange is modified through different mechanisms. On the one hand, erosion might lead to additional CO_2 emissions due to the mineralization of eroded SOC during sediment transport as a result of soil aggregate breakdown (Chappell et al., 2014; Van Hemelryck et al., 2011; Wang et al., 2010). On the other hand, erosion might lead to C sequestration due to the dynamic replacement of SOC at the eroding uplands and the decreased decomposition rate of eroded SOC that is redeposited and buried in flood-plains and lakes (Stallard, 1998; Van Oost et al., 2007). In addition, soil and SOC loss influences terrestrial-atmosphere CO_2 fluxes indirectly by affecting terrestrial productivity, nutrient concentrations in soil and aquatic systems, food webs and optical properties of inland and coastal waters (Beusen et al., 2005; Regnier et al., 2013; Vigiak et al., 2017). To date, many uncertainties still remain in the quantitative assessment of the net effect of large-scale lateral soil and C redistribution on terrestrial-atmosphere CO_2 fluxes (Berhe et al., 2007; Doetterl et al., 2016; Lal, 2003; Liu et al., 2003; Stallard, 1998; Van Oost et al., 2007; Wang et al., 2017). This knowledge gap partly results from the lack of reliable models capable of simultaneously simulating vertical land-vegetation-atmosphere C fluxes and pools, lateral C transport from land to aquatic systems, as well as the interaction between these vertical and lateral C fluxes.

Water erosion and the resulting transport of SOC from land to aquatic systems are still ignored by most land surface models (LSMs) which are used to simulate the exchange of water, energy and C between land and atmosphere, and their evolution in response to climate and anthropogenic land use drivers (Krinner et al., 2005; Kucharik et al., 2000; Sitch et al., 2003). SOC is a C pool that is difficult to represent in LSMs due to the simplified representation of soil biogeochemical processes and the exclusion of some key processes such as erosion-induced lateral C translocation (Borrelli et al., 2017; Doetterl et al., 2016; Todd-Brown et al., 2014). The absence of water erosion-related fluxes in LSMs induces systematic bias in the modeling of regional and global C budgets. The sign and magnitude of this bias is poorly constrained and may range from a 1 Pg C yr^{-1} source of atmospheric CO_2 to a sink of 1 Pg C yr^{-1} (Van Oost et al., 2012; Regnier et al., 2013; Nadeu et al., 2015; Lauerwald et al., 2017; Naipal et al., 2018). One of the main reasons why water erosion processes are not routinely included in LSMs is the high spatial resolution required to represent the effects of topography on overland flow, erosion and sediment redistribution along hillslopes and floodplains (Naipal et al., 2016) and the long time scales involved that would require too much computational resources for integrating this process in a full-fledged LSM.

Soil erosion and the delivery of eroded soil are processes that are highly variable in space and time due to high spatial variability in topography, soil properties, land use and management and the episodic nature of erosive rainfall events. Therefore, current regional erosion and sediment transport models typically rely on forcing data at high spatial and temporal resolution (e.g., 10 to 100 m, 1 min to 1 hr) to represent the lateral soil and C movements (Francesconi et al., 2016; Nearing et al., 1989; Singh et al., 2006). Several large-scale studies have estimated soil erosion and the resulting C loss using high-resolution topography and soil data (Van Oost et al., 2007; Doetterl, Van Oost, & Six, 2012; Borrelli et al., 2018). However, these studies did not represent the temporal evolution of terrestrial ecosystem fluxes as they relied on static vegetation and SOC maps (Table S1 in the supporting information). Naipal et al. (2015, 2016, 2018) went one step further and introduced a scheme that couples a sediment C removal module with biomass and soil C dynamics controlled by climate, CO_2 and land use to simulate the large-scale lateral movement of sediment and C during the last century. However, as the sediment budget module was not embedded into the terrestrial C cycle model (in this case, the ORCHIDEE LSM), this approach cannot account for the feedbacks of soil erosion on the ecosystem C cycle. Tian et al. (2015) developed a scheme that simulates lateral C and nutrient fluxes from land to ocean by coupling a soil erosion model to DLEM (Dynamic Land Ecosystem Model, v2.0). The upgraded DLEM simulates soil and SOC erosion at the high spatial resolution of 5′ (~9 km) for a large-scale LSM, but which still smoothens topographical properties, especially in hilly and mountainous regions.

In this study, the Modified Universal Soil Loss Equation model (MUSLE, Williams, 1975) is dynamically integrated into the ORCHIDEE LSM (Organizing Carbon and Hydrology In Dynamic Ecosystems, Krinner et al., 2005) based on a novel upscaling scheme that allows accounting for topographical and soil heterogeneities at the unprecedentedly high spatial resolution of 3″ (~90 m). The MUSLE model is used to predict event-based sediment discharge (Mg per rainfall event) from the outlets of small water catchments

(Williams, 1975). It was adapted from the original Universal Soil Loss Equation (USLE) approach (Wischmeier & Smith, 1978) by using runoff instead of rainfall intensity and amount to estimate erosion fluxes. Although USLE and its revised version RUSLE (Renard et al., 1997) are widely used soil erosion models, they were developed for estimating the annual gross soil loss from individual slopes, and are thus not well suited to estimate the sediment delivery from headwater basins to river network. Applications of USLE for individual storm events over large areas lead to biases because this model does not explicitly consider runoff, which is a key factor in sediment and C transport (Kinnell, 2005; Odongo et al., 2013; Sadeghi & Mizuyama, 2007). The runoff-based approach of MUSLE partly overcomes this bias and has the additional advantage to be compatible with a LSM that simulates changes in the soil water balance following each rainfall event at relatively high temporal resolution (e.g., half hour). By focusing on the sediment delivery from the outlets of headwater catchments (i.e., gross soil erosion from all hillslopes—soil deposition on footslopes or plains within that headwater catchment), the proposed approach circumvents the need for a detailed representation of the complex and uncertain processes of soil erosion, sediment transport and redeposition along each hillslope.

The main aim of this study is to develop a LSM that can be used to simulate the soil and SOC deliveries from upland ecosystems to rivers and to assess the potential impact of these lateral fluxes on SOC dynamics. For this purpose, the erosion model MUSLE is coupled to the ORCHIDEE LSM. Calibration and evaluation of the coupled ORCHIDEE-MUSLE model (and its upscaling scheme) is achieved by applying it to the Rhine catchment in Central Europe (Figure S1). The Rhine catchment is characterized by contrasted topography, climate and vegetation conditions and has been widely monitored over the past decades. We evaluate the model results with observed runoff data and previous high-resolution model estimates of net soil erosion/deposition rates from Borrelli et al. (2017). Next, we present the simulated spatial and temporal (interannual and seasonal) variations of soil and SOC delivery rates from uplands to the Rhine river. Finally, we quantify the effects of lateral soil and C redistribution on the SOC stock in the Rhine Catchment over the period 1901–2014.

2. Materials and Methods

2.1. ORCHIDEE LSM

ORCHIDEE is a process-based LSM, which is described in detail by Krinner et al. (2005). In short, the core of ORCHIDEE is organized around three models: (1) the SECHIBA model (Ducoudré et al., 1993) that describes the fluxes of energy and water at the interface of atmosphere and land surface, including the soil water dynamics, (2) the STOMATE model (Saclay Toulouse Orsay Model for the Analysis of Terrestrial Ecosystems, Viovy, 1996) that simulates the C fluxes between soil, vegetation, and atmosphere, including processes such as plant phenology, photosynthesis, C allocation, and SOC decomposition, and (3) the dynamic vegetation module inherited from the dynamic vegetation model LPJ (Lund-Potsdam-Jena) (Sitch et al., 2003), which simulates vegetation dynamics such as plant establishment and mortality, light competition and the introduction or elimination of a plant type due to fire or some other lethal environmental conditions.

We selected the ORCHIDEE-SOM version (Version r5039, Camino-Serrano et al., 2018) that provides a depth-dependent description of the production and decomposition of SOC as basis for the development of ORCHIDEE-MUSLE. Following the CENTURY model (Parton et al., 1987), the soil C in ORCHIDEE-SOM is subdivided into two litter pools (metabolic and structural) and three SOC pools (active, slow and passive) that differ in their respective turnover times. The vertical soil profile is described by an 11-layer discretization of a 2 m soil profile (Figure S2), with geometrically increasing layer thickness from top to bottom (Camino-Serrano et al., 2018). Vegetation in ORCHIDEE-SOM is represented by 13 plant functional types (PFT): one PFT for bare soil, eight for forests, two for grasslands, and two for croplands (Krinner et al., 2005). There can be multiple PFTs (up to 13 in the default ORCHIDEE-SOM) growing in 1 pixel of the model although the specific locations of different PFTs in each pixel are not explicitly represented. Area fractions (0–1, unitless) of different PFTs in each of the simulated pixel can be obtained from land cover forcing data every year or simulated by the vegetation dynamic module, depending on the model settings. Plant phenology, canopy photosynthesis, C allocation, litterfall production, and the dynamic of litter and SOC in every pixel are simulated for each PFT separately. The average conditions (e.g., average LAI, living biomass stock,

SOC density) in each pixel are calculated from specific values for each PFT present on that pixel and their corresponding area fractions.

The hydrological processes in ORCHIDEE are simulated at a time step of 30 min (Campoy et al., 2013; Guimberteau et al., 2014). Based on gridded precipitation forcing data at a temporal resolution of 3 hr, ORCHIDEE-SOM first calculates canopy interception and throughfall, the latter being further divided into infiltration and surface runoff through a time-splitting procedure according to Green and Ampt (1911) where the wetting front moves with time through the deep soil layers (D'Orgeval et al., 2008). Soil water balance is controlled by the soil hydraulic properties, climate driven and plant-mediated transpiration and bare soil evaporation. Note that the precipitation forcing data only provides the total precipitation amount for each 3 hr (mm 3 hr^{-1}), but no information about the rainfall intensity for time scales shorter than 3 hr. To better capture the temporal distribution of rainfall and surface runoff, a parameter (PREC_SPRED) has been introduced in the model to distribute the rainfall intensity within each 3 hr period. When PREC_SPRED is set to 1, it is assumed that all of the rainfall in each 3 hr occurs within the first 30 min of the 3 hr period (high rainfall intensity). When PREC_SPRED is set to 6, the rainfall is evenly distributed across the 3 hr (low rainfall intensity). In this study, PREC_SPRD is set to 1, because the simulated runoff in Rhine catchment is closest to observations when the PREC_SPRD is set to 1, compared to the simulation results using a larger PREC_SPRD (see section 3).

Soil hydraulics are simulated based on an 11-layer soil diffusion scheme (Campoy et al., 2013; De Rosnay et al., 2000). In that scheme, the vertical soil water flow is simulated using the Fokker-Planck equation that resolves water diffusion in nonsaturated conditions according to Richards equation (Richards, 1931). The relationships between hydraulic conductivity, volumetric water content and matrix potential are described by the Mualem-Van Genuchten model (Mualem, 1976; Van Genuchten, 1980). The maximum soil water content in the 2 m soil is between 820 kg m^{-2} (coarse and fine classes) and 860 kg m^{-2} depending on soil texture. The saturated hydraulic conductivity has been modified (D'Orgeval et al., 2008) to take into account two properties that have opposite effects on conductivity (Beven, 1984; Beven & Germann, 1982): (1) increased soil compactness with depth and (2) enhanced infiltration capacity due to the presence of vegetation that increases soil porosity in the root zone. Free gravitational drainage in the lowest soil layer occurs when actual soil water content is higher than the residual water content (Campoy et al., 2013). More detailed information about the simulation of hydrological processes in ORCHIDEE can be found in Campoy et al. (2013) and Guimberteau et al. (2014).

2.2. The MUSLE

The MUSLE event-based sediment delivery model (Williams, 1975) is based on a combination of controlling factors describing runoff and catchment characteristics, expressed by

$$Y = a\,(Q\,q)^b\,K\,LS\,C\,P \tag{1}$$

where Y is the sediment delivery (Mg per rainfall event) to rivers from the outlet of a catchment for a given storm event, Q (m^3 per rainfall event) is the volume of surface runoff produced over a catchment during that event, q is the peak flow rate ($m^3\ s^{-1}$) at the outlet of the catchment, K is the soil erodibility factor (Mg $MJ^{-1}\ mm^{-1}$), LS is the slope length and gradient factor (dimensionless), C is the cover management factor (dimensionless), P is the factor of erosion control practice (0–1, dimensionless), and a and b are empirical coefficients.

MUSLE has been used and tested in many different catchments with diverse climate, soil, vegetation and topography conditions around the world (e.g., Sadeghi et al., 2014; Zhang et al., 2009). Compared to more complex erosion models such as WEPP (Nearing et al., 1989) and ANSWERS (Francesconi et al., 2016; Singh et al., 2006), the structure of MUSLE is relatively simple, and its input parameters can be obtained from existing geodata. In addition, the runoff and vegetation factors used in MUSLE can be calculated directly from the daily total runoff volume, daily peak discharge rate, root biomass, litter stocks, and canopy cover as simulated by ORCHIDEE.
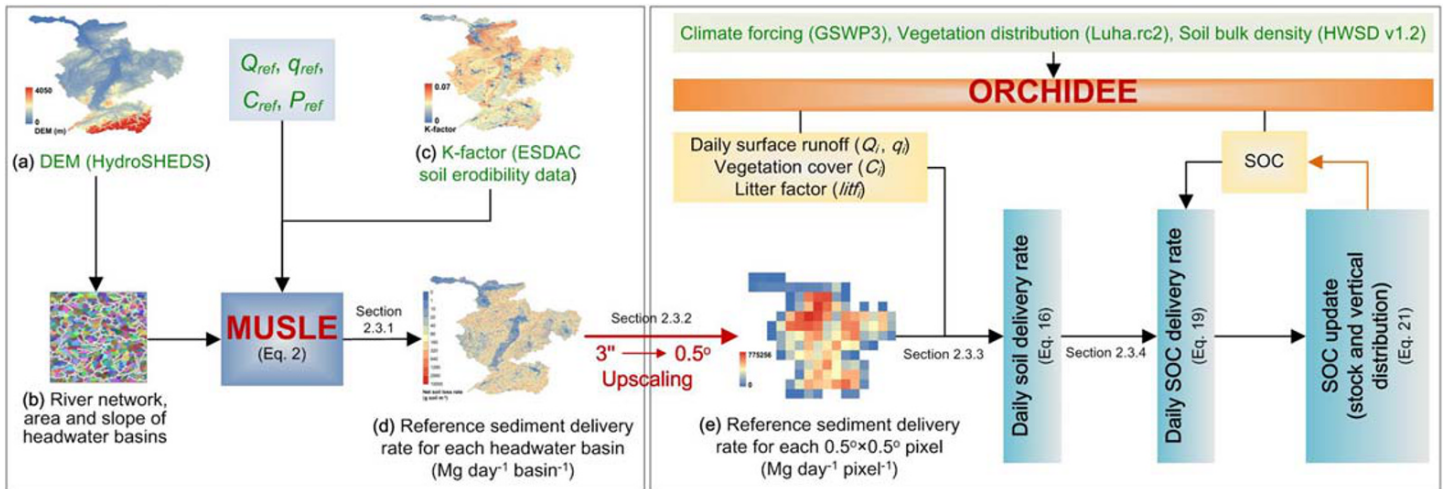
Figure 1. Flowchart for implementing lateral soil and C redistribution processes into the land surface model ORCHIDEE. K factor is the soil erodibility factor ($Mg\ MJ^{-1}\ mm^{-1}$); Q_{ref} is the daily water discharge rate from each water basin ($m^3\ day^{-1}$) under an assumed reference daily runoff condition (reference runoff = 10 mm day^{-1}, Equation 3); q_{ref} is the daily peak flow rate ($m^3\ s^{-1}$) under the assumed reference runoff condition (Equation 5); C_{ref} (=0.1, dimensionless) is the assumed reference cover management factor; P_{ref} (=1.0, dimensionless) is the reference factor for soil conservation practices. See Table 1 for the description of the forcing data (DEM, soil erodibility, climate, vegetation distribution, and soil properties) used in this study.

2.3. Coupling Between ORCHIDEE and MUSLE

The coupled ORCHIDEE-MUSLE was run at 0.5° spatial resolution using the global climate forcing GSWP3 (the Global Soil Wetness Project Phase 3). The applied temporal resolution was the default 30 min time step of ORCHIDEE-SOM for all vertical exchanges of water, C and energy between atmosphere, vegetation, and soils, while the lateral erosion fluxes were simulated at a daily time step. As MUSLE is an event-based erosion model, we assumed that all episodes of rainfalls occurring in the same day belong to one single rainfall event and that the rainfalls occurring in different consecutive days belong to different rainfall events. In what follows, the upscaling strategy required for the ORCHIDEE-MUSLE coupling is described in details.

2.3.1. Sediment Delivery for Reference Conditions

MUSLE is developed to estimate the sediment delivery at the outlet of an individual catchment. We thus applied MUSLE in headwater basins to calculate the sediment delivery from land to the river network, with headwater basins delineated as explained below. First, we extracted the topographic features of each headwater basin in the study area from the high-resolution (3″) digital elevation model (DEM) HydroSHEDS (http://hydrosheds.cr.usgs.gov). We then computed the flow direction (Figure S3b), the flow accumulation (defined by accumulated number of upstream cells, Figure S3c) and the slope steepness (Figure S3e) across the Rhine catchment based on the DEM at 3″ (~90 and 60 m along the latitude and longitude directions, respectively) (Figure S3a) from HydroSHEDS using ESRI's ArcGIS 10.2. The river network (Figure S3d) was then extracted from the flow accumulation map by considering that grid cells with flow accumulation equal to or larger than 1,000, that is a drainage area of approximately 6.5 km^2, belong to the river channel. Using river network and flow direction maps, we then extracted all grid cells that directly discharge into the river network and correspond to the outlets of headwater basins (Figure S3d). Finally, headwater basins (Figure S3d), as well as their drainage area (DA) and average slope steepness (θ) were calculated based on each headwater basin outlet and flow direction. In total (i.e., over the whole Rhine catchment), more than 1.1 million headwater basins with drainage area ranging from less than 0.01 km^2 to more than 6.0 km^2 were extracted.

To scale up the daily sediment delivery computed at the level of headwater basin to the 0.5° grid of ORCHIDEE—a scale required to maintain computational efficiency, we first calculated the daily sediment delivery (Y_{i_ref}, Mg day^{-1}, Figure 1d) in each headwater basin for a given set of reference conditions of runoff and vegetation cover:

$$Y_{i\_ref} = a \left(Q_{i\_ref} \, q_{i\_ref} \right)^b K_i \, LS_i \, C_{ref} \, P_{ref} \tag{2}$$

where Q_{i_ref} is the total water discharge (m³ day⁻¹) at the outlet of headwater basin i for the daily reference runoff condition (R_{ref}) of 10 mm day⁻¹, calculated according to

$$Q_{i\_ref} = 10^{-3} \, R_{ref} \, DA_i \tag{3}$$

$$DA_i = flacc_i \, \Delta lat_i \, \Delta lon_i \tag{4}$$

where DA_i is the drainage area of each headwater basin i (m²), computed from $flacc_i$, the flow accumulation at the outlet of water basin i. Δlat and Δlon are the grid size (m) in latitude and longitude direction. In Equation 2, q_{i_ref} is the daily peak flow rate (m³ s⁻¹) at the headwater basin outlet under the assumed reference runoff condition. Similar to the SWAT model (Soil and Water Assessment Tool, Neitsch et al., 2011), q_{i_ref} was calculated from the maximum 30 min runoff depth and drainage area according to the following equation:

$$q_{i\_ref} = \frac{R_{30\_ref}}{30 \times 60} \left(DA_i^{(d \, DA_i^c)} \right) 1000 \tag{5}$$

where R_{30_ref} (=1 mm 30 min⁻¹) is the assumed daily maximum 30 min runoff. As runoff produced at different locations of a basin does not reach the outlet at the same time, we introduced the parameters c and d to account for the impacts of water convergence on q_{i_ref}. The calibration of those parameters is described in section 2.4.3.

In Equation 2, the term LS_i is the combined dimensionless slope length and steepness factor (Moore & Burch, 1986; Moore & Wilson, 1992) given by

$$LS_i = \left(10^{-6} \frac{DA_i}{22.13} \right)^{0.4} \left(\frac{\sin\theta_i}{0.0896} \right)^{1.3} \tag{6}$$

where θ_i is the average slope steepness of headwater basin i. C_{ref} (0–1, dimensionless) in Equation 2 represents the cover management factor and is set to 0.1 for the reference state. The soil erodibility factor K_i (Mg MJ⁻¹ mm⁻¹) for the Rhine catchment (Figure S3f) was taken from the high-resolution (500 m) soil erodibility data set (Panagos et al., 2014) provided by the European Soil Data Centre (ESDAC). The term P_{ref} was set to 1.0, as we did not consider the impacts of soil conservation practices in reducing soil erosion rate. Note that the choice of reference values for the runoff (R_{ref} and R_{30_ref}), land cover (C_{ref}) and factor of erosion control practice (P_{ref}) does not affect the simulated sediment delivery rate, that is, any set of values would lead to the same result.

2.3.2. Spatial Upscaling Procedure (Reference Conditions)

For the reference state, the total sediment delivery from uplands to the river network in a specific 0.5° × 0.5° pixel k (Y_{k_ref}, Mg day⁻¹) is equal to the sum of sediment delivery from all headwater basins (i) in this pixel:

$$Y_{k\_ref} = \sum_{i=1}^{n} \left(f_{ik} \, Y_{i\_ref} \right) \tag{7}$$

where n is the total number of headwater basins in pixel k and f_{ik} (0–1, dimensionless) is the area fraction of headwater basin i located in pixel k. Combining Equations 2 and 7 allows to generate a map of daily sediment delivery from uplands to the river network at 0.5° spatial resolution (Figure 1e) for the reference conditions of runoff and vegetation cover. This map is then used in ORCHIDEE-MUSLE to simulate the daily sediment delivery as described in the next section.

2.3.3. Daily Sediment Delivery From Uplands to the River Networks (Actual Conditions)

The daily sediment delivery from headwater basins to the river networks (Y_{k_tot}, Mg day⁻¹) at 0.5° spatial resolution for any arbitrary value of runoff and vegetation cover is given by

$$Y_{k\_tot} = \sum_{i=1}^{n}(f_{ik}\, Y_i) = \sum_{i=1}^{n}\left(f_{ik} \sum_{j=1}^{m}\left(a\, (Q_i\, q_i)^{b}\, K_i\, LS_i\, C_{ij}\, vf_{kj}\right)\right) \tag{8}$$

where Y_i (Mg day^{-1}) is the daily sediment delivery from headwater basin i. k and j are the indexes of 0.5° pixel and PFT, respectively. Q_i is the daily total water discharge (m^3 day^{-1}) at the outlet of water basin i, and it is calculated as

$$Q_i = 10^{-3}\, R_k\, DA_i \tag{9}$$

where R_k (mm day^{-1}) is the daily total surface runoff in pixel k simulated by ORCHIDEE-MUSLE at 0.5° spatial resolution every 30 min. We assumed that the surface runoff is evenly distributed in every 0.5° pixel, that is, all headwater basins ($i = 1:n$) in 1 pixel (k) have the same surface runoff ($R_{i\,=\,1:n} = R_k$). In Equation 8, q_i denotes the daily peak flow rate (m^3 s^{-1}) at water basin outlet, calculated from the maximum value of the 48 half-hour runoffs in each day (R_{30_k}, mm 30 min^{-1}):

$$q_i = \frac{R_{30_k}}{30 \times 60}\left(DA_i^{(d\, DA_i^{c})}\right)10^3 \tag{10}$$

Vegetation dynamics in ORCHIDEE are simulated at 0.5° spatial resolution. Thus, all headwater basins in one 0.5° pixel were assigned the same vegetation cover condition. The vegetation in ORCHIDEE is however represented by 13 PFTs ($m = 13$). In Equation 8, the term vf_{kj} (0–1, dimensionless) thus denotes the (evenly distributed) fraction of pixel k covered by each PFT number j ($j = 1:m$). The cover management factor C_{ij} (0–1, dimensionless) in Equation 8 was calculated in ORCHIDEE-MUSLE as a combination of a canopy cover factor ($f\,(vc_{ij})$, 0–1, dimensionless), a litter factor ($f\,(litt_{ij})$, 0–1, dimensionless) and a root factor ($f\,(root_{ij})$, 0–1, dimensionless). As all small headwater basins ($i = 1:n$) located in one 0.5° pixel (k) have the same vegetation cover condition, C_{ij} can be calculated by

$$C_{ij} = f\left(vc_{kj}\right) f\left(litt_{kj}\right) f\left(root_{kj}\right) \tag{11}$$

where $f\,(vc_{kj})$ is calculated from vegetation cover following the method proposed by Yang and Shi (1994) and already applied by, for example, Shi et al. (2004), Zhou et al. (2008), Schönbrodt et al. (2010), and Zhang et al. (2014):

$$f\left(vc_{ij}\right) = \begin{cases} 1.0, & vc_{kj} \leq 0.1 \\ 0.658 - 0.343 log_{10}\left(vc_{kj}\right), & 0.1 < vc_{kj} < 78.3 \\ 0.01, & vc_{kj} \geq 78.3 \end{cases} \tag{12}$$

where vc_{kj} (%) is the canopy cover fraction (equal to the ratio of canopy cover area to the distribution area of each PFT) of PFT j in pixel k. vc_{kj} is updated daily in ORCHIDEE-MUSLE based on the phenology and growing stage of PFT j. Previous studies reported significant impacts of plant litter and plant root in reducing soil erosion (Durán Zuazo & Rodríguez Pleguezuelo, 2008; Li et al., 2014; Poesen et al., 2016). Following the equations implemented in the ANSWERS model (Byne, 1999), the adjustment factor of plant litter ($f\,(litt_{kj})$) and living roots ($f\,(root_{kj})$) are calculated from the litter stock and standing root biomass according to the following equations:

$$f\left(litt_{kj}\right) = e^{-0.56 C_{litt\_kj}/1000} \tag{13}$$

$$f\left(root_{kj}\right) = e^{-0.56 C_{root\_kj}/1000} \tag{14}$$

where C_{litt_kj} (g C m^{-2}) is the sum of aboveground and belowground litter-C stocks in the top seven soil layers (0–19 cm) for PFT j in pixel k, and C_{root_kj} (g C m^{-2}) is the total root biomass. Note that the above-ground biomass in croplands is assumed to be harvested every year and $f\,(litt_{kj})$ for croplands is thus only calculated based on the belowground litter stock.

The daily sediment delivery from uplands to the river network in each 0.5° pixel k was computed for the reference runoff and vegetation cover conditions (Y_{k_ref}) as described in sections 2.3.1 and 2.3.2. We can

now directly calculate the actual daily sediment delivery (Y_{k_tot}) for any other pair of runoff value and vegetation cover characteristics corresponding to a PFT j in pixel k (Y_{kj_tot}, Mg day^{-1}):

$$Ykj\_tot = Y_{k\_ref} \left(\frac{R_k \, R_{30\_k}}{R_{ref} \, R_{30\_ref}} \right)^b \frac{vf_{kj} \, f\left(vc_{kj}\right) f\left(litt_{kj}\right) f\left(root_{kj}\right)}{C_{ref}} \tag{15}$$

This approach has the major advantage that the sediment delivery from headwater basins to the river network is only computed once at the very high spatial resolution of 3″ and is used to scale the sediment delivery for any arbitrary value of runoff and vegetation cover from their reference values. From the PFT-specific total amount of daily sediment delivery (Y_{kj_tot}), the area-averaged sediment delivery rate for a given PFT (NE_{kj}, kg m^{-2} day^{-1}), that is, the net soil loss rate (gross soil erosion—soil deposition on footslopes or plains) from uplands to river channels) can be calculated according to

$$NE_{kj} = \frac{Y_{kj\_tot}}{10^{-3} \, vf_{kj} \, A_k} \tag{16}$$

where A_k (m^2) is the total area of pixel k. The depth of eroded soil per day (Z_{kj}, m day^{-1}) is then obtained by dividing the area-averaged sediment delivery rate by the soil bulk density (BD_{kj}, kg m^{-3}):

$$Z_{kj} = \frac{NE_{kj}}{BD_{kj}} \tag{17}$$

In ORCHIDEE-MUSLE, the depths of the 11 soil layers are fixed (Figure S2). Following soil erosion, some of the soil and C originally located in a given layer will progressively move into the overlying upper soil layer. The deepest, 11th soil layer (bottom soil layer, 1.5–2.0 m) is replenished by subsoil located deeper than 2 m (Figure S2). We assumed that there is no organic C below 2 m, and there is always sufficient soil at depths deeper than 2 m to replenish the soil loss in the surface layers.

2.3.4. Carbon Redistribution and Profile Evolution

Like in the original ORCHIDEE-SOM (Camino-Serrano et al., 2018), SOC in ORCHIDEE-MUSLE is subdivided into three pools (active, slow and passive) and is discretized over 11 soil layers down to 2 m depth. In general, the simulated SOC concentration decreases exponentially from surface to deep soil layers. SOC decomposition is represented by first order kinetics and the decomposition rate depends on the specific turnover rate of each SOC pool. The decomposition process is modulated by soil moisture, temperature, clay content and the "priming effect" of labile organic matter (Camino-Serrano et al., 2018; Guenet et al., 2016). Moreover, the vertical transport of SOC between different soil layers induced by bioturbation is simulated according to a diffusion-type law (Camino-Serrano et al., 2018). Overall, the daily net change of SOC pools in each layer is represented by the mass conservation equation:

$$\frac{dSOC}{dt} = I_C - \tau \, f_a \, SOC + D_C \tag{18}$$

where I_C is the carbon input from decomposed litter or other related donor C pools, f_a is the modulating factor adjusting the decomposition rate based on soil temperature, moisture, texture (clay content) as well as the priming effect of fresh C input (Guenet et al., 2016, 2018) and D_C is the net SOC exchange with adjacent soil layers through vertical transport induced by bioturbation.

The daily area-averaged SOC delivery rate from each headwater basin to the river network (equal to the delivery rate of particulate organic C (POC)) induced by soil erosion is simulated based on the average SOC concentration in the top seven soil layers (0–19 cm). For PFT j in pixel k, the SOC delivery rate (NE_C_{kj}) is calculated by

$$NE\_C_{kj} = \frac{Z_{kj}}{Z_7} SOC7_{kj} \tag{19}$$

$$SOC7_{kj} = \sum_{l=1}^{7} SOC_{kjl} \tag{20}$$

Table 1
Source and Spatial Resolution of the Main Forcing and Validation Data Used in This Study

Data		Resolution	Source
Forcing	Climate	0.5°	GSWP3[a]
	Vegetation cover	0.5°	LUHa.rc2[b]
	Soil bulk density	0.5°	HWSD v1.2[c]
	DEM	3″	HydroSHEDS[d]
	Soil erodibility	500 m	Panagos et al. (2014)
Validation	Net soil erosion/deposition rate	100 m	Borrelli et al. (2018)
	Runoff discharge	Site observation	GRDC[e]
	SOC stocks	30″	HWSD v1.2[c]
		5′	GSDE (Shangguan et al., 2014)
		1 km	OCTOP (Jones et al., 2005)

[a]https://www.isimip.org/gettingstarted/details/4/;   [b]http://luh.umd.edu/readme_LUHa_v1.shtml;   [c]FAO/IIASA/ISRIC/ISSCAS/JRC, 2012 (https://webarchive.iiasa.ac.at/Research/LUC/External-World-soil-database/HTML/); [d]http://hydrosheds.cr.usgs.gov;   [e]https://www.bafg.de/GRDC/EN/Home/homepage_node.html

where $SOC7_{kj}$ (g C m^{-2}) denotes the sum of SOC stock in the top seven soil layers. Z_7 is the depth at the bottom of the seventh soil layer (0.19 m) and SOC_{kjl} is the SOC content (g C m^{-2}) of layer l.

We assumed that the amount of SOC eroded from each of the top seven soil layers is positively related to the pool size of the corresponding soil layer. As a result of the loss in surface soil, part of the SOC that was originally stored in deeper soil layers will be transported up the sediment column and eventually exposed to erosion if it reaches the surface soil layers. This migration process of SOC in a soil layer l of PFT j in pixel k is simulated according to

$$SOC_{kjl\_new} = \begin{cases} \left(\left(1 - \dfrac{Z_{kj}}{Z_7} \right) SOC7_{kj} + \dfrac{Z_{kj}}{Z_8 - Z_7} SOC_{kj8} \right) \dfrac{SOC_{kjl}}{SOC7_{kj}} , & l \leq 7 \\[2ex] \left(1 - \dfrac{Z_{kj}}{Z_l - Z_{l-1}} \right) SOC_{kjl} + \dfrac{Z_{kj}}{Z_{l+1} - Z_l} SOC_{kj(l+1)} , & 8 \leq l \leq 10 \\[2ex] \left(1 - \dfrac{Z_{kj}}{Z_l - Z_{l-1}} \right) SOC_{kjl} , & l = 11. \end{cases} \quad (21)$$

where SOC_{kjl_new} (g C m^{-2}) is the updated SOC stock in soil layer l (lay_l) of the pixel k. Note that the vertical evolution of the SOC profile is simulated separately for each of three SOC pools of differing reactivity (active, slow and passive).

2.4. Model Evaluation
2.4.1. Study Area
ORCHIDEE-MUSLE was calibrated and evaluated at the regional scale of the Rhine catchment (Figure S1), which is characterized by a drainage area of about 1.6×10^5 km^2. The elevation and slope steepness vary drastically in Rhine catchment (Figure S3). In the northern and central plains, the elevation is generally lower than 100 m and the slope steepness is mostly less than 1°. In the mountainous regions, especially the Alps, the elevation can be above 3,000 m and slope steepness can be larger than 30°. A large fraction of the catchment is under the influence of a temperate climate with mean annual precipitations varying between 600 mm in central Rhine and 2,500 mm in the Alps (Van Dijk & Kwaad, 1998). The main land use types consist of forest (35%), crop land (22%), grass land (39%) and urban area (4%), and the land cover has changed extensively during the past decades (Hurkmans et al., 2009).

2.4.2. Forcing Data and Model Protocol
The meteorological forcing data used for our simulations were obtained from the global reanalysis product of the Global Soil Wetness Project Phase 3 (GSWP3, Table 1). The GSWP3 data set contains globally gridded data of near surface wind, air temperature, humidity, air pressure, incoming short-wave and long-wave radiation, rainfall and snowfall rates for the period 1901 to 2014 on a 3-hourly time step at 0.5° resolution (http://forge.ipsl.jussieu.fr/orchidee/wiki/Documentation/Forcings). Every year during the whole simulation period since 1901, the vegetation distribution was dynamically prescribed using PFT maps obtained

from the LUHa.rc2 data set (Land Use History). Soil type was defined based on Zobler (1999). Soil bulk density was taken from the HWSD database (Harmonized World Soil Database v1.2, FAO/IIASA/ISRIC/ISSCAS/JRC, 2012).

Daily sediment and SOC delivery from headwater basins to the river network was simulated at 0.5° spatial resolution yet with the upscaling from 1.1 million headwater catchments over the period 1901–2014. Before launching this historical simulation, ORCHIDEE-MUSLE was run over a "spin-up" period of 10,000 yr starting from "bare ground" (with zero vegetation and SOC content) until the SOC pools reached a steady state. During the "spin-up" period, the meteorological data, PFT maps and atmospheric CO_2 concentrations from 1901 to 1910 were used repeatedly to drive the model. Moreover, in order to assess the impacts of erosion-induced soil loss on the land C cycle in Rhine catchment, we also ran the default ORCHIDEE-SOM model (Version r5039) following exactly the same modeling protocol. The impact of erosion on the SOC balance was quantified by comparing the model outputs from ORCHIDEE-SOM and ORCHIDEE-MUSLE.

2.4.3. Calibration and Validation

Although several studies already estimated the gross soil erosion rates in the Rhine catchment or across Europe (Cerdan et al., 2010; Naipal et al., 2016, 2018; Panagos et al., 2015), to our knowledge, only a few studies have estimated the sediment delivery from uplands to the river network (Van Dijk & Kwaad, 1998; Asselman, 1999; Borrelli et al., 2018). In this study, the gridded product of net soil erosion/deposition rate (erosion minus deposition, in Mg ha^{-1} yr^{-1}) from ESDAC (Table 1, Borrelli et al., 2018) was used to calibrate the model parameters a, b, c, and d in Equations 1, 2, 5, 8, and 10 and to evaluate the simulated results. The ESDAC product provides the net soil erosion/deposition rate across all European Union countries using the land cover map of 2010 at 100 m spatial resolution, as simulated by the WaTEM/SEDEM model using high-resolution data of land cover, soil erodibility, topography and rainfall. This product has been extensively calibrated and validated against observed sediment fluxes from 24 European catchments (Borrelli et al., 2018).

As the net soil erosion/deposition rates from the ESDAC product (100 m) and ORCHIDEE-MUSLE (0.5°) are simulated at quite different spatial resolutions, the parameters a, b, c, and d (Equations 2, 5, 8, and 10) were calibrated here against the area-averaged sediment delivery rates in 28 subcatchments of the Rhine (Figure S1). The area of the 28 subcatchments ranges from less than 500 to 13,600 km^2. The four subcatchments that are mainly located in Switzerland were excluded because ESDAC product only provides the estimate of net soil erosion/deposition rates in European Union countries. For the ESDAC product, the area-averaged sediment delivery rate in a specific subcatchment is calculated by averaging the net soil erosion/deposition rates for all 100 × 100 m grid cells within that subcatchment. For ORCHIDEE-MUSLE, we first calculated the area-averaged sediment delivery rate at the headwater basin scale (NE_i, kg m^{-2} day^{-1}, Figure S4) by

$$NE_i = \left(\frac{Y_{i\_ref}}{Y_{k\_ref}} \sum_{j=1}^{m} \left(Y_{kj\_tot} \right) \right) / DA_i \tag{22}$$

Then, the area-averaged sediment delivery rate for each of the 28 subcatchment of the Rhine (Figure S1) was calculated as the mean value (weighted by the drainage area of each headwater basin) of all headwater basins within each subcatchment.

We used the "leave-one-out" cross-validation method (Tramontana et al., 2016) to evaluate the simulated area-averaged sediment delivery rate, and quantify uncertainties in the parameters a, b, c, and d. The cross validation was conducted 28 times according to the following procedure: Each time, the area-averaged sediment delivery rates in 27 subcatchments were used to calibrate parameters, and the subcatchment excluded in the calibration was then taken as the validation sample. Parameter optimization was performed using the shuffled complex evolution (SCE) algorithm developed by Duan et al. (1993, 1994), which has been proven to be effective for global optimization in many previous studies (e.g., Franchini et al., 2009; Muttil & Jayawardena, 2008). The root-mean-square error (RMSE, Equation 23) between sediment delivery rates obtained from the ESDAC product and the simulated results from the ORCHIDEE-MUSLE was used as the objective metrics, and parameter values that minimize the RMSE were regarded as optimal.

$$RMSE = \sqrt{\left(\frac{\sum_{isub=1}^{n}(NE_{isub\_WS} - NE_{isub\_OM})^2}{n}\right)} \qquad (23)$$

where n ($n = 28$) is the number of training samples, NE_{isub_WS} and NE_{isub_OM} (kg m^{-2} yr^{-1}) are the area-averaged sediment delivery rates in subcatchment *isub* simulated by WaTEM/SEDEM (subscript WS) and ORCHIDEE-MUSLE (subscript OM), respectively. We also used the area-averaged sediment delivery rates for all of the 28 subcatchment together as training samples to optimize an average value of a, b, c, and d. All simulation results shown in section 3 are based on parameters ($a = 43.79$, $b = 0.50$, $c = -0.048$, $d = 1.78$) calibrated against area-averaged sediment delivery rates of the 28 subcatchments together, unless specified otherwise.

The simulated runoff from ORCHIDEE-MUSLE was evaluated against observed annual water discharge (m^3 yr^{-1}) at 14 hydrological gauging stations corresponding to variable drainage areas (Figure S1). The gauging data were extracted from the Global Runoff Data Centre (GRDC, 56068 Koblenz, Germany). The simulated SOC stocks were evaluated against the SOC stocks from three spatially gridded soil databases: the Harmonized World Soil Database (HWSD, v1.2), the Topsoil Organic Carbon Content for Europe (OCTOP, Jones et al., 2005), and the Global Soil Dataset for use in Earth System Models (GSDE, Shangguan et al., 2014).

2.4.4. Analysis of Uncertainties

Based on the 28 cross validations and the calibration using all subcatchments together as training samples, we obtained 29 sets of parameter values a, b, c, and d. By comparing these parameter values, we estimated the mean and standard deviation of parameters a (40.58 ± 5.81), b (0.51 ± 0.014), c (-0.053 ± 0.010), and d (1.91 ± 0.26). The spread in values was then used to quantify uncertainties in simulated area-averaged sediment delivery rates induced by the parameter uncertainties.

Uncertainties arising from the land cover forcing data were quantified by comparing the LUHa.rc2 used in this study to the CORINE land cover data (https://land.copernicus.eu). The CORINE land cover was developed by image analysis and land use/cover digitalization of Landsat photos in a GIS environment. The data are available in a raster format at a pixel resolution of 100 m, and correspond to the years 1990, 2000, 2006, and 2012 (the data for 1990 was not used here as it excludes the upper part of the Rhine Catchment located in Switzerland). Validation of the CORINE land cover data for Europe relies on extensive field surveys and results indicate that the achieved accuracy exceeds 85% (Buttner, 2014). Note that there are 45 land cover types in the original CORINE data set. We thus developed a lookup table (Table S2 in the supporting information) to reclassify these 45 land cover types into the 13 PFTs of ORCHIDEE. More detailed information about the CORINE land cover data can be found in Panagos et al. (2015).

To simulate the sediment delivery rate using the high-resolution CORINE land cover maps, we first calculated the fractions of different PFTs in each 0.5° pixel according to the CORINE data product. Then, the resulting land cover data, was used in combination with the daily runoff (Equation 15) and vegetation factors (Equation 11, for each PFT) simulated by ORCHIDEE-MUSLE to drive the MUSLE (Equation 8) to perform a CORINE-based simulation of the daily sediment delivery rate from uplands to river networks in each 0.5° pixel. In our model, the land cover conditions of all headwater basins that belong to the same 0.5° pixel are also assumed to be identical. To explore the uncertainties in simulated sediment delivery rate caused by the averaging of land cover conditions at 0.5° spatial scale, we conducted a simulation where the land cover composition in each headwater basin is specified according to the high-resolution CORINE land cover map. We then compared the so-derived sediment delivery rates to the sediment delivery rates simulated using the average land cover condition of each 0.5° pixel.

Uncertainties in the soil erodibility (K) data used in this study have already been estimated by Panagos et al. (2014). We thus used their results to discuss the potential uncertainties in our simulation results caused by the soil erodibility. Panagos et al. (2015) have also estimated the factor of erosion control practice (e.g., contour farming, stone walls and grass margins) at the European scale. We used their estimates to quantify the P factor in the Rhine catchment, as well as the potential uncertainties arising from this factor in our model.
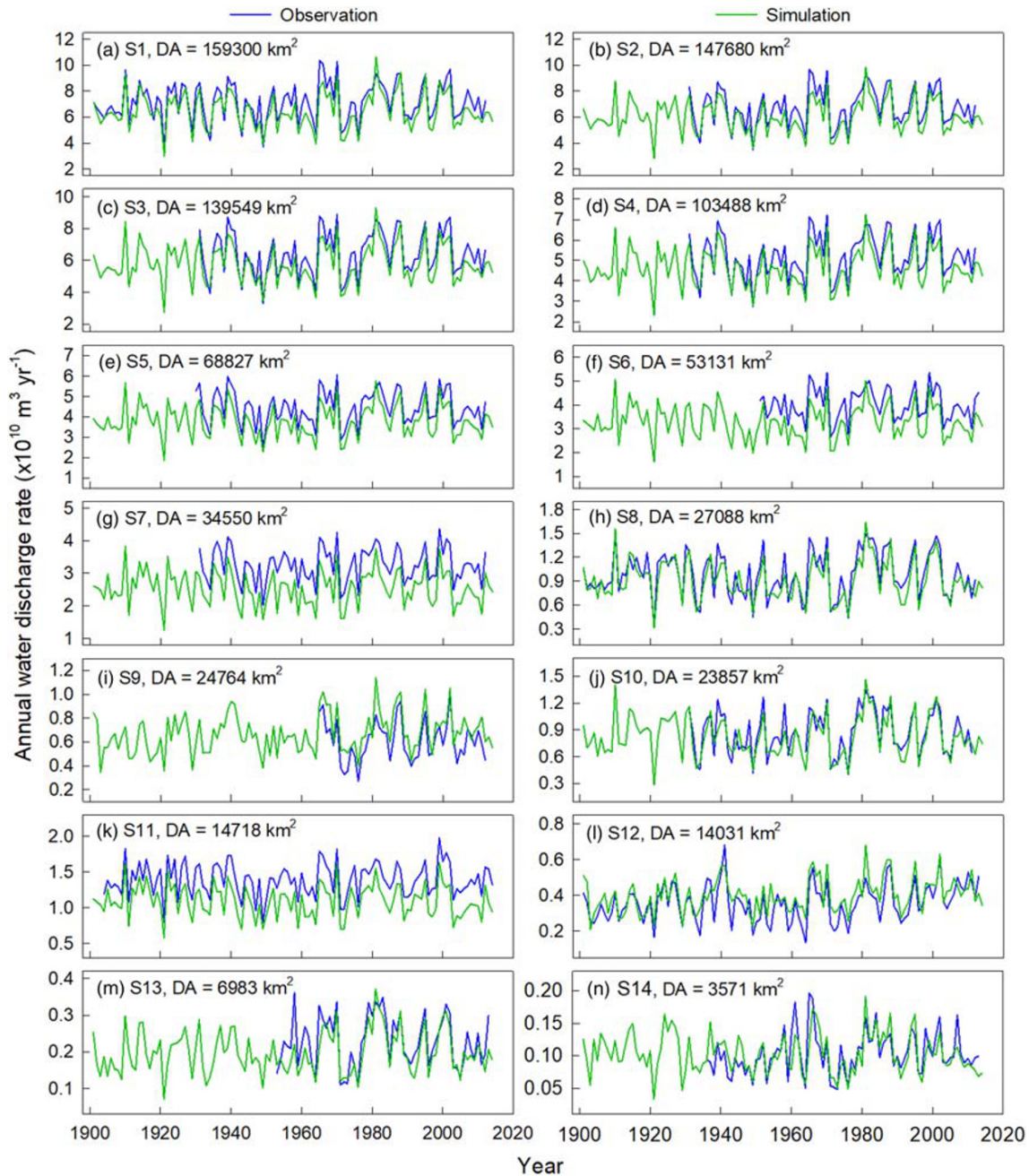
Figure 2. Comparison of simulated (green) and observed (blue) annual water discharge at 14 gauging stations in the Rhine watershed. DA denotes the drainage area of each gauging station.

3. Results and Discussion

3.1. Model Evaluation

Comparison of simulated and observed annual water discharge indicates that ORCHIDEE-MUSLE can reproduce the magnitude and interannual variations of runoff at gauging stations capturing different drainage areas (Figure 2). For most of the 14 gauging stations, ORCHIDEE-MUSLE explains more than 80% of the interannual variation in runoff during the period 1901–2014 (Figure S5). At site S1 located close to the estuary of the Rhine River and draining the entire catchment area, 86% of the interannual variations
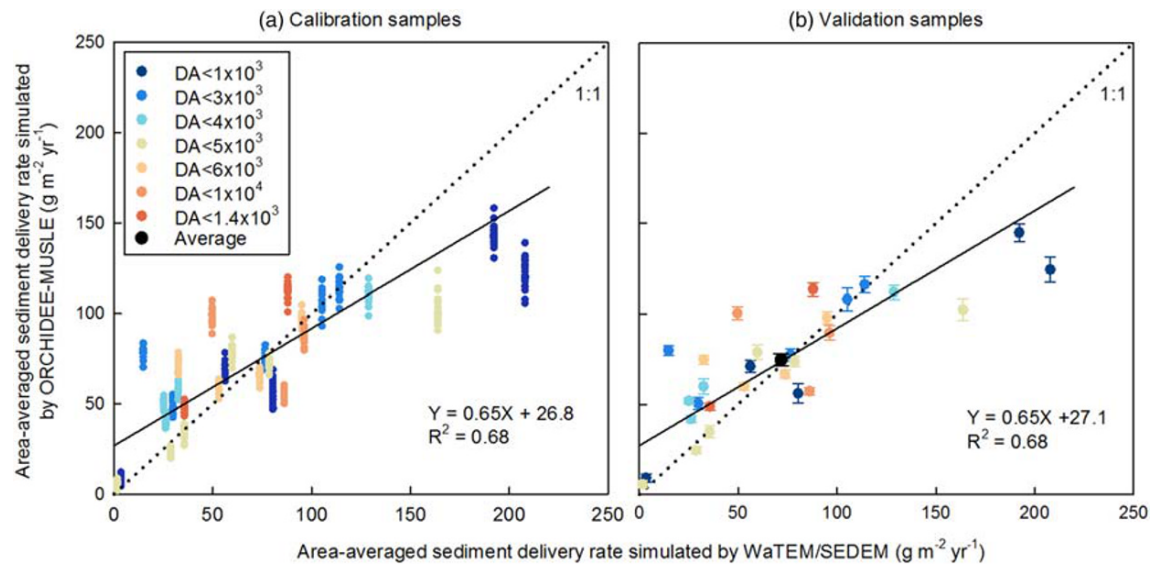
Figure 3. Comparison of the area-averaged sediment delivery rates from uplands to the river network simulated by WaTEM/SEDEM and by ORCHIDEE-MUSLE for 28 subcatchments of the Rhine (excluding the four subcatchments in Switzerland). DA denotes the drainage area of different subcatchments (km^2). The black dot in figure (b) denotes the simulated average sediment delivery rate in all of the 28 subcatchments. The solid line is the regression line of simulation results from ORCHIDEE-MUSLE against WaTEM/SEDEM. Error bars denote the uncertainties in the simulated sediment delivery rates caused by the uncertainties of parameters a, b, c, and d in Equations 1, 2, 5, and 10.

of water discharge are explained by the simulation results (Figure S5). On average, the simulated annual water discharge at site S1 is 6.5×10^{10} ($\pm 1.4 \times 10^{10}$, standard deviation representing interannual variation) $m^3 \, yr^{-1}$, which is only 9% lower than the observed value (7.2×10^{10} ($\pm 1.4 \times 10^{10}$) $m^3 \, yr^{-1}$).

The simulated area-averaged sediment delivery rates from uplands to the river network in different subcatchments of the Rhine using ORCHIDEE-MUSLE are overall comparable to those of WaTEM/SEDEM (Figures 3 and S6). The relative biases between the two models are generally lower than 30%, with larger biases occurring mostly in the smaller subcatchments (<5,000 km^2). For all of the 28 subcatchments of the Rhine (excluding the four subcatchments in Switzerland, Figure S6), the average sediment delivery rate estimated in our study is 74.6 (± 3.3) $g \, m^{-2} \, yr^{-1}$, which is close to the estimated value by WaTEM/SEDEM (71.7 $g \, m^{-2} \, yr^{-1}$). Although the biases in simulated average sediment delivery rates are large in several small subcatchments (Figure 3), they have very limited impact on the estimation error for the total yearly soil delivery over the whole Rhine catchment ($9.1 \pm 0.4 \, Tg \, yr^{-1}$, Figure S6). In other words, the estimation errors for the large subcatchments mainly determine the overall estimation accuracy over the Rhine catchment (Figure S6).

Comparison of simulated SOC stocks from ORCHIDEE-MUSLE and SOC stocks from the HWSD and OCTOP soil databases indicates that the model overestimates the SOC stocks (in the top 30 cm or 1 m soil layer) in the central portion of the Rhine catchment, while it underestimates the SOC stocks in the northern and southern parts (Figures 4 and S7–S9). In contrast, when the GSDE is used as benchmark, ORCHIDEE mostly underestimates SOC stocks in the whole Rhine catchment (Figures 4c and 4f). These results indicate that SOC stock estimates from soil databases are already quite uncertain, as already pointed out by Tifafi et al. (2018). Not surprisingly, the SOC stocks simulated by ORCHIDEE-MUSLE are generally lower than those obtained with ORCHIDEE-SOM without erosion (Figures S7d, S7e, S8c, and S8d) due to the effects of erosion removal in the former model version (Figure 5).

3.2. Spatiotemporal Dynamics of Sediment and SOC Delivery Rates

The sediment and SOC delivery rates from headwater basins to the river network show large spatial variations across the Rhine catchment (Figure 5). From the Southeast to the Northwest portions of the catchment and largely following the S-N gradient from steeper to flatter topography, the sediment delivery rates decrease from more than 3 $g \, C \, m^{-2} \, yr^{-1}$ to less than 0.05 $g \, C \, m^{-2} \, yr^{-1}$. On average, the annual sediment
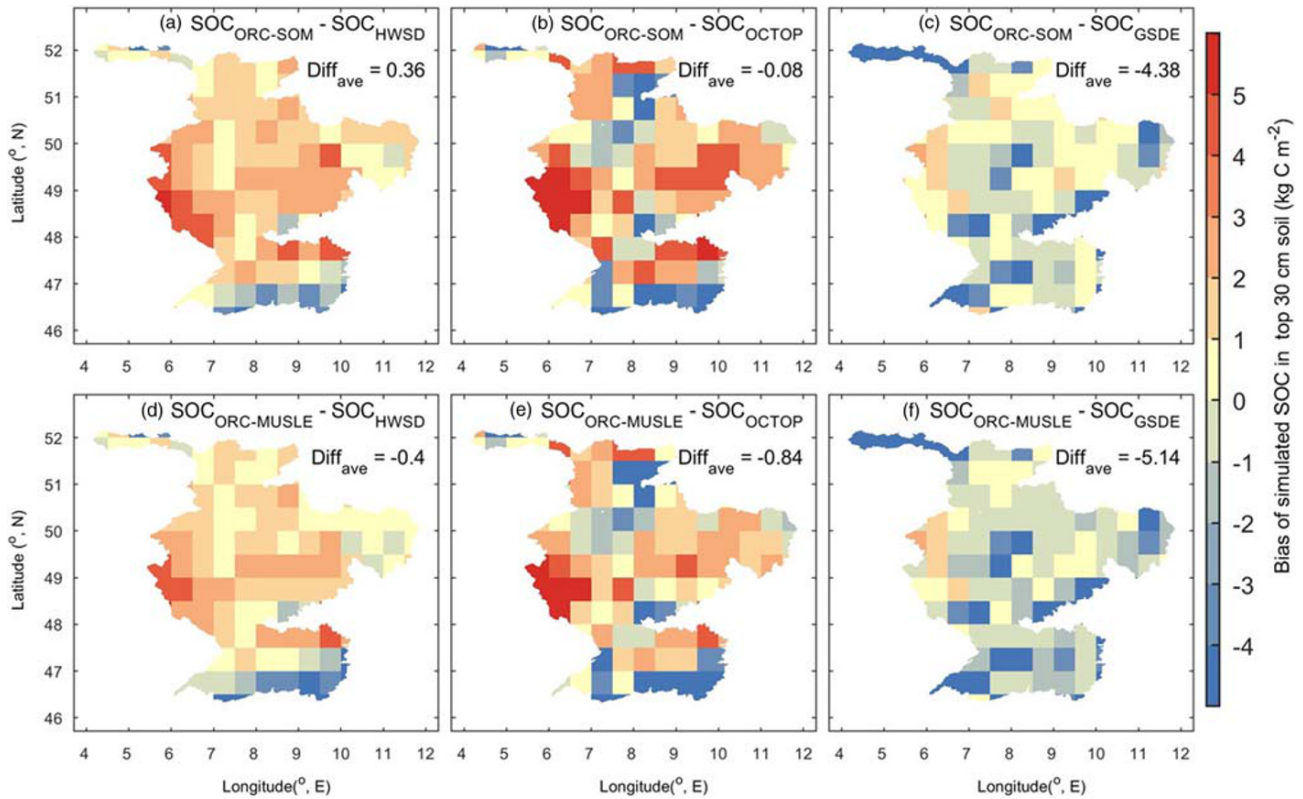
Figure 4. Difference between observed SOC stocks in the top 30 cm soil layer extracted from three large-scale soil databases (SOC_{HWSD} from HWSD v1.2, FAO/IIASA/ISRIC/ISSCAS/JRC, 2012; SOC_{OCTOP} from OCTOP, Jones et al., 2005; and SOC_{GSDE} from GSDE, Shangguan et al., 2014) and simulated values from the default ORCHIDEE-SOM ($SOC_{ORC-SOM}$, a, b, c) and the upgraded ORCHIDEE-MUSLE ($SOC_{ORC-MUSLE}$, d, e, f) models. Red colors (positive values) indicate an overestimation while blue colors (negative values) indicate an underestimation by the models. $Diff_{ave}$ is the average difference between SOC stocks extracted from soil databases and the simulated values for the entire Rhine catchment.

and SOC delivery rates across the entire Rhine catchment are 107.1 g m^{-2} yr^{-1} and 1.19 g C m^{-2} yr^{-1}, respectively. The higher value reported here compared to the one reported above (74.6 g C m^{-2} yr^{-1}) stems from the contribution of the four Swiss subcatchments.

The seasonal dynamics in sediment delivery rates are mainly controlled by runoff (Figure 6a) and vegetation growth (Figure 6b), with values generally higher in winter and spring and lower in summer and autumn (Figure 6c). The highest monthly sediment delivery rate (2.83 Tg month^{-1}) during the period 1901–2014
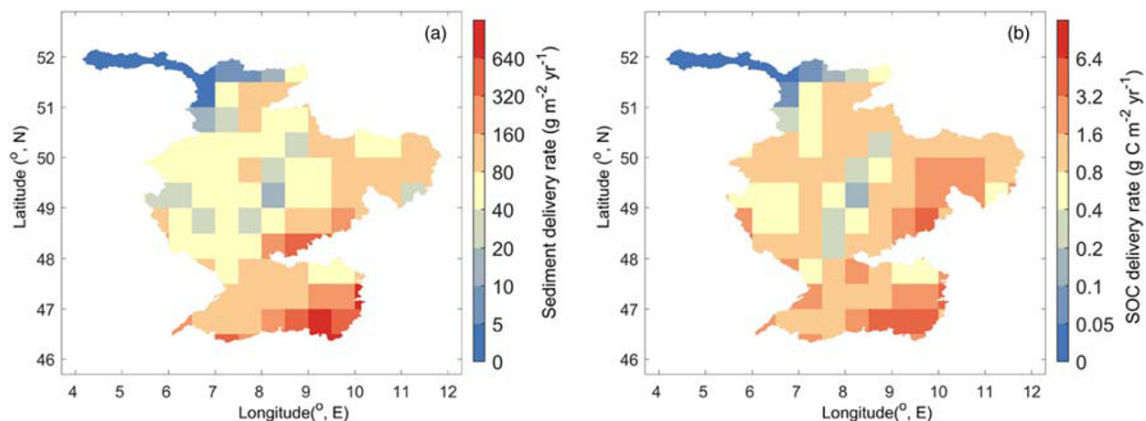

Figure 5. Spatial distributions of simulated average sediment (a) and soil organic carbon (SOC, b) delivery rates from uplands to the river network of the Rhine during the period 1901–2014.
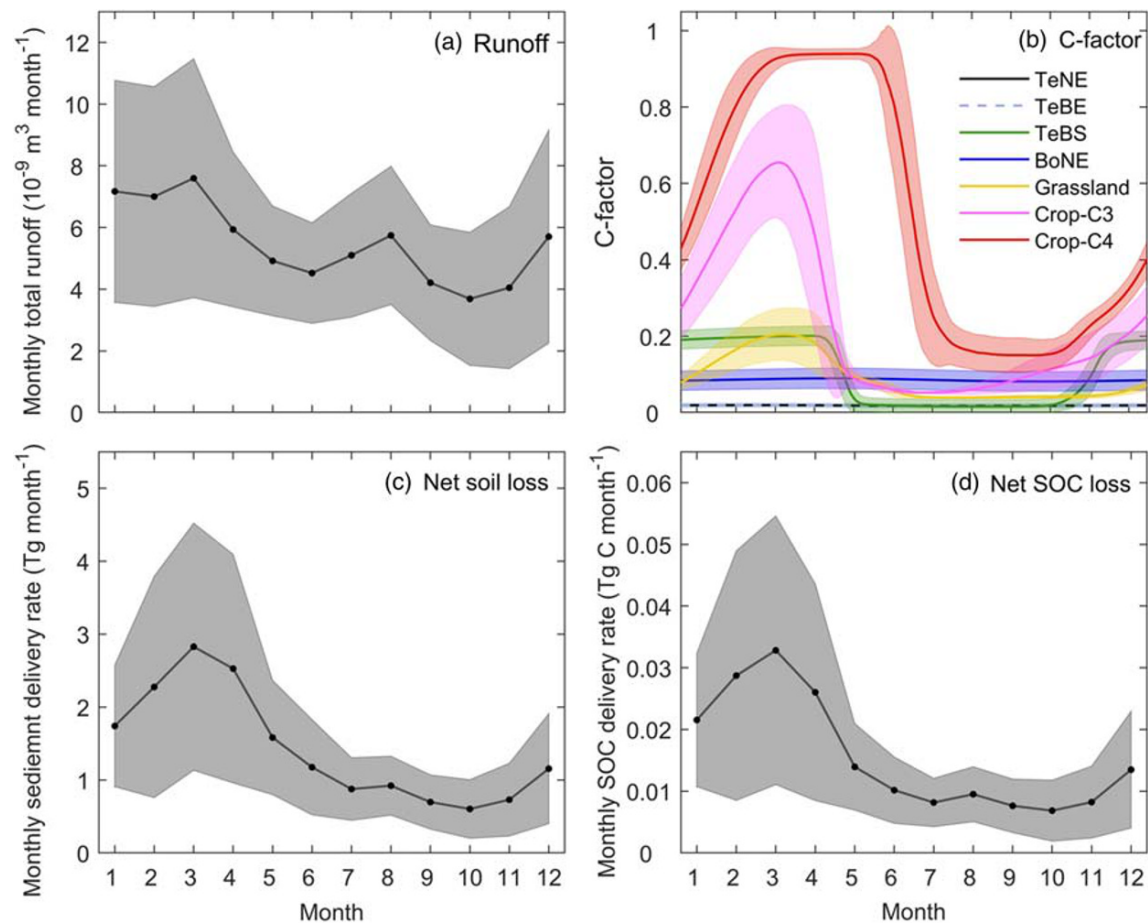
Figure 6. Seasonal dynamics of average runoff (a), revised C factor (b, Equation 11), and sediment and SOC delivery rates from uplands to river network (c, d) in the whole Rhine catchment. The line with dots denotes the average value for the period from 1901 to 2014. The shaded area denotes the standard deviation of interannual variations. TeNE: temperate needle-leaved evergreen forest; TeBE: temperate broadleaved evergreen forest; TeBS: temperate broadleaved summer-green forest; BoNE: boreal needle-leaved evergreen forest; C3 and C4: crops using C3 and C4 photosynthesis pathways, respectively. Note that the runoff, sediment, and SOC delivery rates shown in the figure correspond to the sum of these variables over all 0.5° pixels within the Rhine catchment, but not the water, sediment, and SOC delivery from the outlet of the Rhine catchment.

occurs in March and is more than four times larger than the minimum value found in October (0.60 Tg month^{-1}). The net SOC delivery rates follow the same seasonal pattern, with higher values in winter and spring compared to summer and autumn (Figure 6d).

From 1901 to 2014, the annual sediment and SOC delivery rates from uplands to the river network of the Rhine declined significantly (Figure 7). The annual total runoff in the Rhine catchment varies between years, but it does not show a significant trend over the last century that could explain this decline (Figure 7a). In contrast, land use has changed substantially over the last century. Many croplands were transformed to grasslands during the period 1901–1940, followed by transformations from croplands and grasslands into forests during the period 1940–1960. After 1960, the same transformations were pursued but at a significantly slower pace (Figure 7b). The abandonment of croplands, which have a higher sediment delivery rate than forests and grasslands, largely explains why the annual sediment delivery rate in the catchment has decreased significantly from about 20 Tg yr^{-1} at the beginning of the twentieth century to 13 Tg yr^{-1} in recent years (Figure 7c). Despite abandonment, croplands remain the main contributors to the total sediment delivery during the entire simulation period, from about 58% in 1901–1910 to 42% in 2001–2014. The contribution of forest to total sediment delivery increased from 6% in 1910s to 18% in 2000s due to the expansion of forest area, while the contribution of grasslands increased from 36% to 40% over the same period. The interannual dynamics of SOC delivery rate, as well as the percentages of SOC delivery rates from croplands, grasslands and forests are overall similar to those of sediment delivery rates (Figure 7d).
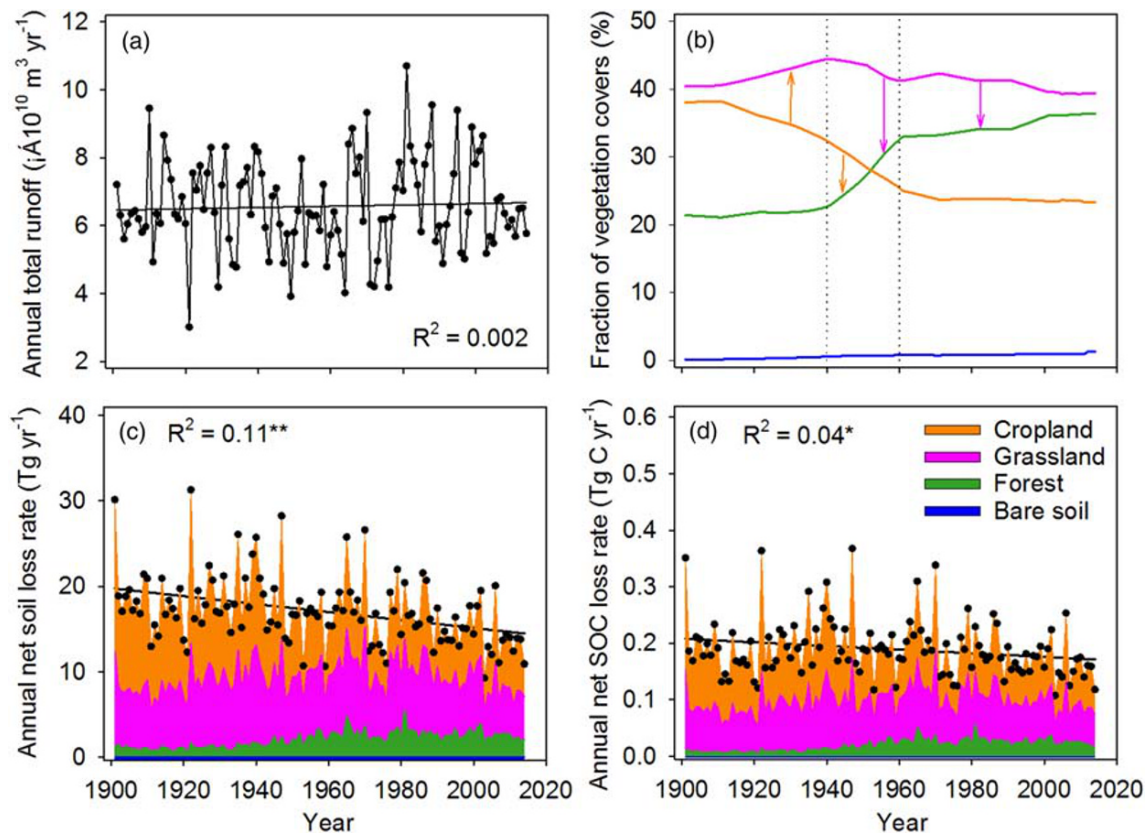
Figure 7. Interannual variations in total runoff (a), vegetation cover (b), and annual sediment and SOC delivery rates from uplands to river network (c, d) in the Rhine catchment from 1901 to 2014. * and ** denotes significant ($p < 0.05$) and very significant ($p < 0.01$) changes in the trend, respectively. Black dots in (c) and (d) indicate total sediment and SOC delivery rate, respectively.

Our results show that ORCHIDEE-MUSLE is a useful tool to estimate the impacts of seasonal vegetation dynamics and changing rainfall regimes on sediment and C delivery from soils to rivers, and further on the SOC budget of a large catchment. This is an advantage over complex, mechanistic erosion models (Francesconi et al., 2016; Nearing et al., 1989; Singh et al., 2006) which are only applicable for single small catchments, due to the limitations of data needed for model parameterization and the considerable computation workloads. In the past two decades, a growing number of large-scale soil erosion-C cycle models have been developed (Bouchoms et al., 2017; Chappell et al., 2016; Liu et al., 2003; Lugato et al., 2016; Naipal et al., 2016, 2018; Van Oost et al., 2005; Zhang et al., 2014). However, most of these models are run at a time step of 1 year or even a decade (Rosenbloom et al., 2001), and thus cannot represent the impacts of seasonal vegetation and event-based rainfall dynamics on C erosion and river delivery. In ORCHIDEE-MUSLE, vegetation growth is updated daily and litter dynamics are simulated at a half-hour time step. Therefore, our model can represent temporal changes resulting from the variability in vegetation cover on soil erosion in detail. The hydrological processes (e.g., evapotranspiration, infiltration and surface runoff) in ORCHIDEE-MUSLE are also simulated at half-hourly time step. Besides the total amount of daily surface runoff, the daily maximum half-hourly runoff that reflects rainfall intensity to a certain degree is also an important factor accounted for in our sediment delivery model (Equations 8, 10, and 15). Therefore, our model can be used to study the impacts of changes in rainfall regimes (e.g., changes in rainfall frequency and intensity induced by climate change) on lateral C transfers.

3.3. Effects of Large-Scale Soil Erosion on Soil C Balance

Comparison of simulated equilibrium SOC stocks from ORCHIDEE-SOM and ORCHIDEE-MUSLE reveals that the soil and SOC deliveries from headwater basins to the river network lead to substantial changes in the land C balance of the Rhine catchment (Figure 8). The erosion-induced decrements of equilibrium SOC stocks range from less than 0.1 kg C m^{-2} to more than 3 kg C m^{-2} locally (Figure 8a). On average, our
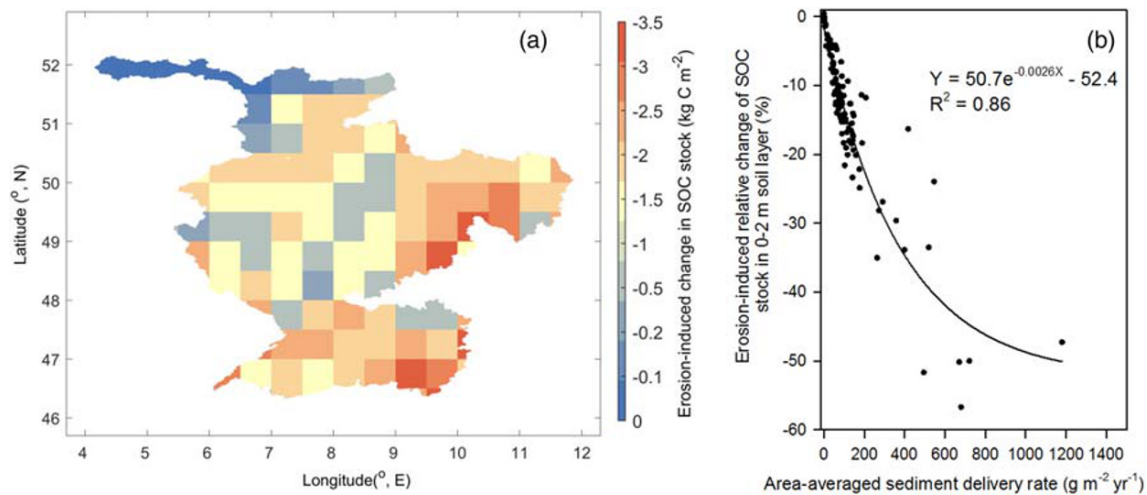
Figure 8. Changes in equilibrium SOC stocks (calculated as the difference between SOC stocks in 2014 simulated by ORCHIDEE-MUSLE and ORCHIDEE-SOM) caused by lateral soil and carbon movement (a); relationship between sediment delivery rate and erosion-induced relative changes in SOC stocks (b).

simulation results show that an increment of 100 g m^{-2} yr^{-1} in the sediment delivery rate results in a 5.7% decrease in the SOC stock (Figure 8b).

Further statistics indicate that although the average annual SOC delivery (1.19 g C m^{-2} yr^{-1}) from headwater basins to the river network represents about 0.5% of the annual net vegetation production (234.7 g C m^{-2} yr^{-1}) and 0.01% of the total SOC stock in the top 2 m soil layer (10.4 kg C m^{-2}), long-term soil erosion in the Rhine catchment has the potential to cause a 12.4% reduction in the total top 2 m SOC stocks. The erosion of surface SOC and exposure of former subsoil SOC are assumed to induce a reduction of SOC stock (Lal, 2003; Doetterl, Six, et al., 2012; Wang et al., 2014). However, there are also studies arguing that the erosion-induced reduction of SOC stock might be limited because the eroded SOC can be dynamically replaced by new litter-C input unless the erosion rates are large enough to offset plant productivity (Berhe et al., 2007; Harden et al., 1999). Our results suggest that even when the reductions in vegetation productivity and plant litterfall caused by soil erosion are ignored (impacts of soil erosion on soil nutrient availability and vegetation growth are not represented in the current version of ORCHIDEE-MUSLE), soil erosion over a long period of time (e.g., hundreds to thousands of years) can still result in a significant ($p < 0.01$) reduction (12.4% in the Rhine catchment) in the equilibrium SOC stock (Figures 8 and S7).

The incorporation of MUSLE into the ORCHIDEE-SOM LSM through a computationally efficient upscaling scheme (see section 2.3.1) appears to be an effective strategy to simulate erosion-induced sediment and SOC delivery rates from uplands to river networks at the large spatial scale typically used for global LSM applications. The processes of soil erosion and sediment delivery imperatively need to account for the spatial variability in topography and soil properties at a scale of tens to hundreds of meters, as those environmental controls have a strong and nonlinear effect on erosion rates (Bouchoms et al., 2017; Kirkels et al., 2014; Morgan et al., 1998; Van Rompaey et al., 2010). LSMs resolve rainfall and runoff at high temporal resolution (Krinner et al., 2005; Sitch et al., 2003), which is of advantage when simulating the event-dependent magnitude of erosion processes. However, LSMs are generally run at relatively coarse spatial resolutions (e.g., 0.5°) determined by the resolution of global climate forcing data sets and CPU limitations. In this study, the implementation of erosion processes based on our upscaling scheme that accounts for the fine-scale effects of topography induces only a 40% increase in the computation time of ORCHIDEE. In contrast, if the model had been run directly at the 3″ spatial resolution of the topography data, the number of grid cells represented in the model would increase by a factor of 360,000, which would entrain a similar increase in computation costs and in the storage capacity.

3.4. Model Uncertainties
3.4.1. Uncertainties in Forcing Data
Biases in the land cover and soil erodibility forcing files, as well as the lack of constrains regarding erosion control practices induce uncertainties in the simulation results. Land cover conditions provided by the

LUHc.v2 data set is obviously different from that provided by the CORINE data set (Figure S10). For the whole Rhine catchment, the grassland fraction (0.39) in the LUHc.v2 data set is higher than in the CORINE data set (0.18). The forest (0.34) and cropland (0.26) fractions extracted from the LUHc.v2 data set, however, are lower than those (forest: 0.38, cropland: 0.31) extracted from the CORINE data set. Biases in the LUHc.v2 land cover data impact the simulated sediment delivery rates (Figure S11) and for the whole Rhine catchment, the average value (102.6 g m^{-2} yr^{-1}) for the years 2000, 2006 and 2012 combined is about 9% higher than the estimation based on the CORINE data set (93.2 g m^{-2} yr^{-1}). In some specific pixels of the Rhine catchment, the relative differences between both land cover products can even exceed 40% in absolute terms (Figure S11d). Uncertainties in sediment delivery rates caused by the upscaling of land cover conditions from headwater basin scale to the scale of a 0.5° pixel are significantly smaller (Figure S12). Our analysis indicates that the relative differences between sediment delivery rates simulated assuming average land cover condition in each 0.5° pixel and that simulated using the actual CORINE land cover data for each headwater basin are generally smaller than 5% in absolute terms. Integrated over the entire Rhine catchment, the sediment delivery rate simulated with average land cover conditions for each 0.5° pixel (93.2 g m^{-2} yr^{-1}) is almost same to that simulated at the headwater basin scale (93.4 g m^{-2} yr^{-1}).

Uncertainties in soil erodibility data have been estimated by Panagos et al. (2014). Compared to soil erodibility studies performed at smaller scales across Europe (e.g., Bakker et al., 2008; de Moor & Verstraeten, 2008; Tetzlaff et al., 2013), the estimate of Panagos et al. (2014) shows an average deviation of ±14.3%. As the sediment delivery rate simulated by MUSLE is linearly related to the soil erodibility factor (Equation 1), the sediment delivery rate simulated here, and which rely on the Panagos data set, is also potentially biased by ±14.3%. In our model, the effects of soil conservation practices, which would decrease erosion rates, are also ignored. However, the study of Panagos et al. Study of Panagos, Borrelli, Meusburge, Alewell, et al. (2015), based on extensive observations from the Land Use/Cover Area frame Statistical survey (LUCAS) in 2012, suggests that areas with soil conservation practices only cover 14.7% the whole Rhine catchment, and only in 1.6% of these areas, soil conservation practices have been found to decrease soil erosion rates by 20% or more (Figure S13). For the whole Rhine catchment, these results suggest that soil conservation practices may only decrease total soil erosion by less than 3% (Figure S13). Thus, excluding soil conservation practices should have limited impact in our simulations.

Even though the spatial (0.5°) and temporal (3 hr) resolutions of the precipitation forcing data used in this study can be considered high-resolution for global-scale LSM runs, the precipitation forcing data can still introduce uncertainties in simulated sediment delivery rates. Many observations have revealed that both rainfall amount and intensity show strong spatial variability, especially in hilly and mountainous regions (e.g., Ballabio et al., 2017; Isotta et al., 2013; Rysman & Lemaitre, 2016). The precipitation forcing data at 0.5° spatial resolution thus cannot represent the rainfall variability at the smaller scale of headwater basins. Moreover, the climate forcing data used in this study only provides the total rainfall amount (mm) every 3 hr, but no information is available regarding the rainfall distribution within these 3 hr periods. Therefore, although the hydrological module of ORCHIDEE runs at a half-hour time step and the parameter PREC_SPRED (=1) allows to tune the rainfall intensity (see section 2.1 for details) at the 30 min time scale, the simulated daily total runoff (Q) and daily peak flow rate (q) could still be biased compared to the real values.

3.4.2. Uncertainties in Model Parameters

Uncertainties in model parameters and in empirical functions used to calculate the runoff (Equations 5 and 10) and vegetation (Equations 11–14) factors of MUSLE induce some uncertainties in our simulation results. Peak flow rate at the outlet of a water basin is closely related to the drainage area and shape, average slope, the Manning's roughness and the depth of surface runoff (Ascough et al., 1995; Williams, 1995). The process-based functions for calculating peak flow rate are complex and hard to parameterize and calibrate for large-scale applications (Ascough et al., 1995). In this study, we introduced a simple empirical function of drainage area and depth of the maximum half-hour runoff (Equations 5 and 10) to calculate the peak flow rate. Our analysis indicates that the uncertainties in parameters a, b, c, and d (Equations 1, 2, and 5) used to calculate the runoff factors (Q and q) of MUSLE may lead to a 3–15% change in simulated sediment delivery rates compared to the "baseline run" (see section 2.4.3), depending on the subcatchment (Figures 3 and S6). For the whole Rhine, uncertainties in these four parameters result in up to 10% variation in average sediment delivery rate. Another source of uncertainty arises from the equation applied to constrain the

canopy cover factor in MUSLE (Equation 12). Equation 12 has been developed based on observations in a subcatchment of the Yangtze River in China. Although more than 200 soil erosion rates measured from 30 runoff-erosion plots under both natural and simulated rainfall events have been included to calibrate that equation, there might still be some biases when applying it to other river basins.

3.4.3. Uncertainties in Model Algorithm

Uncertainties also arise from the model structure itself, in particular in the way the erosion-induced vertical SOC profile is updated. In ORCHIDEE-MUSLE, the simulation of, for example, hydrological processes, litter and carbon decomposition, root vertical distribution depend on an 11-layer discretization scheme of the soil column down to 2 m depth. In our scheme, we assumed that there is no organic C in the subsoil deeper than 2 m, and that the depth of soil layer deeper than 2 m is always larger than the depth of eroded soil. This is a simplification as in many areas where the depth of the erodible soil layer is larger than 2 m, there is still a certain amount of SOC in the deep soil (>2 m), although the SOC concentrations are in general very small (Jobbagy & Jackson, 2000). In addition, the soil erosion rates in some catchments with steep slopes, low vegetation cover or high frequency of storms can be significantly higher than the local soil formation rates (Pimentel, 2006; Verheijen et al., 2009). After a long time (e.g., hundreds to thousands of years) of soil erosion, there will thus be very little or even no erodible soil in these catchments. Application of our model in catchments with high soil erosion rate but shallow erodible soil layer over long timescales may thus overestimate sediment and SOC delivery rates. In this study, we applied ORCHIDEE-MUSLE for 114 yr. As the annual sediment delivery rates in Rhine subcatchments are generally lower than 300 g m^{-2} yr^{-1} (~0.3 mm yr^{-1}, Figure 5a), the depths of total eroded soil from 1901–2014 in most areas should be lower than 3.5 cm. Therefore, our assumption that there is always enough erodible soil is a reasonable approximation for this study.

Unknown small-scale heterogeneity of vegetation cover, topographic condition and soil erodibility within headwater basins might also generate uncertainties in our simulation results. Different from spatially distributed erosion models (e.g., WEPP, Nearing et al., 1989) which explicitly simulate the gross soil erosion from slopes and the delivery of eroded soil from slopes to catchment outlets through the channel network (i.e., the connectivity between slope and river), MUSLE is a spatially lumped model which directly simulates the sediment delivery from catchment outlets (Williams, 1975) based on a combination of controlling factors including runoff, vegetation, soil erodibility and topographic characteristics. Although extensive studies have proved the effectiveness of MUSLE in simulating the sediment delivery rates based on average land cover conditions and topographic properties (e.g., slope steepness) of the whole catchment (e.g., Sadeghi et al., 2014; Zhang et al., 2009), other studies have shown that the spatial distribution of vegetation cover or geomorphic units can strongly affect the sediment and flow connectivity between slopes and river channel (Borselli et al., 2008; Heckmann et al., 2018), in addition to the fractions of each vegetation cover and the average slope steepness. Moreover, the SOC delivery rates (for each vegetation type) are calculated based on the average sediment delivery rate in each 0.5° pixel, rather than on the sediment delivery rate in each headwater basin. This might also induce biases in the simulated SOC fluxes. Finally, croplands in ORCHIDEE are represented in a simplified way by classifying crops into two groups (the C3 crop and C4 crop) based on their photosynthesis characteristics. Therefore, ORCHIDEE might not be able to accurately capture the seasonal dynamics of planting, canopy growth rate and harvest for all crop types.

3.5. Model Limitations

As described before, soil erosion can alter land-atmosphere C exchange by influencing vegetation productivity; however, this feedback mechanism has not yet been included in the current version of ORCHIDEE-MUSLE. Vegetation production directly determines the ability of terrestrial ecosystems to absorb atmospheric CO_2 as well as the inputs of plant litter to soil (Bouchoms et al., 2019; Frankenberg et al., 2011; Melillo et al., 1993; Schimel, 2010; Sitch et al., 2008). As soil erosion can significantly alter soil nutrient availability (e.g., nitrogen (N) and phosphorus (P)), soil water holding capacity and soil structure and texture, it might have a significant impact on vegetation productivity (Lal, 2010; Larson et al., 1983; Quine & Zhang, 2002). Recently, terrestrial N and P cycles have already been incorporated into the ORCHIDEE model (Goll et al., 2017; Zaehle et al., 2010). By coupling ORCHIDEE-MUSLE and the ORCHIDEE branches that simulate terrestrial N and P cycling (e.g., ORCHIDEE-CNP, Goll et al., 2017), it will be possible to

develop a more comprehensive LSM that can simulate the feedbacks of soil erosion on vegetation productivity and the erosion-induced N and P fluxes along the land-ocean continuum.

We also showed that ORCHIDEE-MUSLE is able to capture the sediment and C delivery from uplands to inland waters, but the transport and deposition processes of sediment and C in floodplains and river networks are not represented. The fate of eroded SOC that is eroded and delivered to rivers directly affects land-ocean and land-atmosphere C fluxes (Lal, 2003; Regnier et al., 2014; Smith & Buddemeier, 2005). Mineralization of particulate organic C during the transport process in river will increase aquatic CO_2 emission and decrease the C flux from land to ocean, as already shown for dissolved organic carbon (Bowring et al., 2019; Hastie et al., 2019; Lauerwald et al., 2017). Particulate organic C redeposited on flat slopes, floodplains, deltaic or waterlogged environments (e.g., lakes, reservoirs and coastal oceans) however can be preserved for a long time and results in a long-term increase of land C storage (Chappell et al., 2014; Hoffmann et al., 2013; Smith et al., 2001; Stallard, 1998; Wang et al., 2010). A logical next step in terms of model development will be to include the transport, deposition and decomposition processes of particulate organic C in aquatic systems into our model for estimating the lateral C movements and their impacts on land-atmosphere C exchange more accurately and comprehensively.

4. Conclusions

In this study, we introduced an upscaling scheme for coupling the soil erosion model MUSLE, which simulates the sediment delivery from headwater basins, into the LSM ORCHIDEE-SOM, which represents the terrestrial C cycle at regional to global scales. Our modeling strategy allows including a wide range of temporal scales affecting erosional fluxes, from event-based and seasonal variability to multicentennial trends in sediment deliveries. Application and evaluation of the upgraded model ORCHIDEE-MUSLE to the Rhine catchment proves that our model reproduces the spatiotemporal variation in river runoff and sediment delivery rates from uplands to the river network. Our simulation results reveal that at centennial time scale, soil erosion induces a significant reduction in simulated SOC stocks. Ignoring soil erosion—as done in traditional LSMs—leads to significant overestimation of regional SOC accumulation. Furthermore, according to our simulations sediment and SOC delivery rates have decreased significantly over the period 1901–2014, mainly due to a conversion of croplands to forests.

To our knowledge, this is the first attempt to incorporate high-resolution (3″) erosion and lateral C redistribution into a LSM by using an upscaling scheme that calculates the sediment delivery from small headwater catchments before aggregating them to the coarse resolution of the LSM. Even though several uncertainties remain, we show that this is a promising approach to incorporate lateral particulate C fluxes from land to ocean into LSMs. In order to give a more accurate and comprehensive evaluation on the role of lateral C redistribution within the global C cycle, it is necessary to further calibrate our model for other river catchments and incorporate missing but essential processes into our model such as the fate of particulate organic C delivered to the river network, the C dynamics in floodplains and aquatic sediments, and the feedbacks of soil erosion on vegetation productivity.

Data Availability Statement

The source code of ORCHIDEE-MUSLE model developed in this study is available online (https://forge.ipsl.jussieu.fr/orchidee/browser/branches/publications/ORCHIDEE-MUSLE-r6129) from 22 July 2019. All forcing and validation data used in this study are publicly available online. The specific websites for these data can be found in section 2.4.

References

Ascough, I. J. C. II, Baffaut, C., Nearing, M. A., & Flanagan, D. C. (1995). Watershed model channel hydrology and erosion processes. In D. C. Flanagan & M. A. Nearing (Eds.), *USDA Water Erosion Prediction Project: Hillslope profile and watershed model documentation* (Chap. 13, Vol. 13, pp. 4–9). West Lafayette, Indiana: National soil Erosion research laboratory, USDA Agricultural Research Service.

Asselman, N. E. M. (1999). Suspended sediment dynamics in a large drainage basin: the River Rhine. *Hydrological Processes*, *13*, 1437–1450.

Bakker, M. M., Govers, G., van Doorn, A., Quetier, F., Chouvardas, D., & Rounsevell, M. (2008). The response of soil erosion and sediment export to land-use change in four areas of Europe: The importance of landscape pattern. *Geomorphology*, *98*(3–4), 213–226. https://doi.org/10.1016/j.geomorph.2006.12.027

Ballabio, C., Borrelli, P., Spinoni, J., Meusburger, K., Michaelides, S., Begueria, S., et al. (2017). Mapping monthly rainfall erosivity in Europe. *The Science of the Total Environment*, *579*, 1298–1315. https://doi.org/10.1016/j.scitotenv.2016.11.123

Berhe, A. A., Harte, J., Harden, J. W., & Torn, M. S. (2007). The significance of the erosion-induced terrestrial carbon sink. *Bioscience*, *57*(4), 337–346. https://doi.org/10.1641/B570408

Beusen, A. H. W., Dekkers, A. L. M., Bouwman, A. F., Ludwig, W., & Harrison, J. (2005). Estimation of global river transport of sediments and associated particulate C, N, and P. *Global Biogeochemical Cycles*, *19*, GB4S05. http://doi.org/10.1029/2005GB002453

Beven, K. (1984). Infiltration into a class of vertically non-uniform soils. *Hydrological Sciences Journal*, *29*(4), 425–434. https://doi.org/10.1080/02626668409490960

Beven, K., & Germann, P. (1982). Macropores and water flow in soils. *Water Resources Research*, *18*(5), 1311–1325. https://doi.org/10.1029/WR018i005p01311

Borrelli, P., Robinson, D. A., Fleischer, L. R., Lugato, E., Ballabio, C., Alewell, C., et al. (2017). An assessment of the global impact of 21st century land use change on soil erosion. *Nature Communications*, *8*(1), 2013. http://doi.org/10.1038/s41467-017-02142-7

Borrelli, P., Van Oost, K., Meusburger, K., Alewell, C., Lugato, E., & Panagos, P. (2018). A step towards a holistic assessment of soil degradation in Europe: Coupling on-site erosion with sediment transfer and carbon fluxes. *Environmental Research*, *161*, 291–298. https://doi.org/10.1016/j.envres.2017.11.009

Borselli, L., Cassi, P., & Torri, D. (2008). Prolegomena to sediment and flow connectivity in the landscape: A GIS and field numerical assessment. *Catena*, *75*(3), 268–277. https://doi.org/10.1016/j.catena.2008.07.006

Bouchoms, S., Wang, Z., Vanacker, V., Doetterl, S., & Van Oost, K. (2017). Modelling long-term soil organic carbon dynamics under the impact of land cover change and soil redistribution. *Catena*, *151*, 63–73. https://doi.org/10.1016/j.catena.2016.12.008

Bouchoms, S., Wang, Z., Vanacker, V., & Van Oost, K. (2019). Evaluating the effects of soil erosion and productivity decline on soil carbon dynamics using a mode-based approach. *The Soil*, *5*, 367–382. https://doi.org/10.5194/soil-5-367-2019

Bowring, S. P. K., Lauerwald, R., Guenet, B., Zhu, D., Guimberteau, M., Regnier, P., et al. (2019). ORCHIDEE MICT-LEAK (r5459), a global model for the production, transport and transformation of dissolved organic carbon from Arctic permafrost regions, Part 2: Model evaluation over the Lena River basin. *Geoscientific Model Development Discussion*, 1–45. https://doi.org/10.5194/gmd-2018-322

Buttner, G. (2014). CORINE land cover and land cover change products. *Remote Sensing and Digital Image Processing*, *18*, 55–74. https://doi.org/10.1007/978-94-007-7969-3_5

Byne, F. W. (1999). *Predicting sediment detachment and channel scour in the process-based planning model ANSWERS-2000*. Blacksburg, VA: M.S. thesis, Virginia Tech.

Camino-Serrano, M., Guenet, B., Luyssaert, S., Ciais, P., Bastrikov, V., De Vos, B., et al. (2018). ORCHIDEE-SOM: Modeling soil organic carbon (SOC) and dissolved organic carbon (DOC) dynamics along vertical soil profiles in Europe. *Geoscientific Model Development*, *11*, 937–957. https://doi.org/10.5194/gmd-11-937-2018

Campoy, A., Ducharne, A., Cheruy, F., Hourdin, F., Polcher, J., & Dupont, J. C. (2013). Response of land surface fluxes and precipitation to different soil bottom hydrological conditions in a general circulation model. *Journal of Geophysical Research: Atmospheres*, *118*, 10,725–10,739. https://doi.org/10.1002/jgrd.50627

Cerdan, O., Govers, G., Le Bissonnais, Y., Van Oost, K., Poesen, J., Saby, N., et al. (2010). Rates and spatial variations of soil erosion in Europe: A study based on erosion plot data. *Geomorphology*, *122*(1-2), 167–177. https://doi.org/10.1016/j.geomorph.2010.06.011

Chappell, A., Baldock, J., & Sanderman, J. (2016). The global significance of omitting soil erosion from soil organic carbon cycling schemes. *Nature Climate Change*, *6*(2), 187–191. https://doi.org/10.1038/nclimate2829

Chappell, A., Webb, N. P., Viscarra Rossel, R. A., & Bui, E. (2014). Australian net (1950s–1990) soil organic carbon erosion: Implications for CO_2 emission and land–atmosphere modelling. *Biogeosciences*, *11*, 5235–5244. https://doi.org/10.5194/bg-11-5235-2014

Ciais, P., Borges, A. V., Abril, G., Meybeck, M., Folberth, G., Hauglustaine, D., & Janssens, I. A. (2008). The impact of lateral carbon fluxes on the European carbon balance. *Biogeosciences*, *5*(5), 1259–1271. https://doi.org/10.5194/bg-5-1259-2008

Cole, J. J., Prairie, Y. T., Caraco, N. F., McDowell, W. H., Tranvik, L. J., Striegl, R. G., et al. (2007). Plumbing the global carbon cycle: Integrating inland waters into the terrestrial carbon budget. *Ecosystems*, *10*(1), 172–185. https://doi.org/10.1007/s10021-006-9013-8

D'Orgeval, T., Polcher, J., & de Rosnay, P. (2008). Sensitivity of the West African hydrological cycle in ORCHIDEE to infiltration processes. *Hydrological Earth System Science*, *12*, 1387–1401.

de Moor, J. J. W., & Verstraeten, G. (2008). Alluvial and colluvial sediment storage in the Geul River catchment (the Netherlands)—Combining field and modelling data to construct a Late Holocene sediment budget. *Geomorphology*, *95*(3–4), 487–503. https://doi.org/10.1016/j.geomorph.2007.07.012

De Rosnay, P., Bruen, M., & Polcher, J. (2000). Sensitivity of surface fluxes to the number of layers in the soil model used in GCMs. *Geophysical Research Letters*, *27*, 3329–3332. https://doi.org/10.1029/2000GL011574

Doetterl, S., Berhe, A. A., Nadeu, E., Wang, Z., Sommer, M., & Fiener, P. (2016). Erosion, deposition and soil carbon: A review of process-level controls, experimental tools and models to address C cycling in dynamic landscapes. *Earth-Science Reviews*, *154*, 102–122. https://doi.org/10.1016/j.earscirev.2015.12.005

Doetterl, S., Six, J., Van Wesemael, B., & Van Oost, K. (2012). Carbon cycling in eroding landscapes: Geomorphic controls on soil organic C pool composition and C stabilization. *Global Change Biology*, *18*(7), 2218–2232. https://doi.org/10.1111/j.1365-2486.2012.02680.x

Doetterl, S., Van Oost, K., & Six, J. (2012). Towards constraining the magnitude of global agricultural sediment and soil organic carbon fluxes. *Earth Surface Processes and Landforms*, *37*(6), 642–655. https://doi.org/10.1002/esp.3198

Drake, T. W., Raymond, P. A., & Spencer, R. G. M. (2018). Terrestrial carbon inputs to inland waters: A current synthesis of estimates and uncertainty. *Limnology and Oceanography Letters*, *3*(3), 132–142. https://doi.org/10.1002/lol2.10055

Duan, Q., Sorooshian, S., & Gupta, V. K. (1994). Optimal use of the SCE-UA global optimization method for calibrating watershed models. *Journal of Hydrology*, *158*(3-4), 265–284. https://doi.org/10.1016/0022-1694(94)90057-4

Duan, Q. Y., Gupta, V. K., & Sorooshian, S. (1993). Shuffled complex evolution approach for effective and efficient global minimization. *Journal of Optimization Theory and Applications*, *76*(3), 501–521. https://doi.org/10.1007/BF00939380

Ducoudré, N. I., Laval, K., & Perrier, A. (1993). SECHIBA, a new set of parameterizations of the hydrologic exchanges at the land-atmosphere interface within the LMD atmospheric general circulation model. *Journal of Climate*, *6*(2), 248–273. https://doi.org/10.1175/1520-0442(1993)006<0248:SANSOP>2.0.CO;2

Durán Zuazo, V. H., & Rodríguez Pleguezuelo, C. R. (2008). Soil-erosion and runoff prevention by plant covers. A review. *Agronomy for Sustainable Development*, *28*(1), 65–86. https://doi.org/10.1051/agro:2007062

FAO/IIASA/ISRIC/ISSCAS/JRC (2012). Harmonized World Soil Database (Version 1.2), Rome, Italy and IIASA, Laxenburg, Austria: FAO.

Francesconi, W., Srinivasan, R., Pérez-Miñana, E., Willcock, S. P., & Quintero, M. (2016). Using the Soil and Water Assessment Tool (SWAT) to model ecosystem services: A systematic review. *Journal of Hydrology*, *535*, 625–636. https://doi.org/10.1016/j.jhydrol.2016.01.034

Franchini, M., Galeati, G., & Berra, S. (2009). Global optimization techniques for the calibration of conceptual rainfall-runoff models. *Hydrological Sciences Journal*, *43*, 443–458.

Frankenberg, C., Fisher, J. B., Worden, J., Badgley, G., Saatchi, S. S., Lee, J. E., et al. (2011). New global observations of the terrestrial carbon cycle from GOSAT: Patterns of plant fluorescence with gross primary productivity. *Geophysical Research Letters*, *38*, L17706. https://doi.org/10.1029/2011GL048738

Galy, V., Peucker-Ehrenbrink, B., & Eglinton, T. (2015). Global carbon export from the terrestrial biosphere controlled by erosion. *Nature*, *521*(7551), 204–207. https://doi.org/10.1038/nature14400

Goll, D. S., Vuichard, N., Maignan, F., Jornet-Puig, A., Sardans, J., Violette, A., et al. (2017). A representation of the phosphorus cycle for ORCHIDEE (revision 4520). *Geoscientific Model Development*, *10*(10), 3745–3770. https://doi.org/10.5194/gmd-10-3745-2017

Guenet, B., Camino-Serrano, M., Ciais, P., Tifafi, M., Maignan, F., Soong, J. L., & Janssens, I. A. (2018). Impact of priming on global soil carbon stocks. *Global Change Biology*, *24*(5), 1873–1883. https://doi.org/10.1111/gcb.14069

Guenet, B., Moyano, F. E., Peylin, P., Ciais, P., & Janssens, I. A. (2016). Towards a representation of priming on soil carbon decomposition in the global land biosphere model ORCHIDEE (Version 1.9.5.2). *Geoscientific Model Development*, *9*(2), 841–855. https://doi.org/10.5194/gmd-9-841-2016

Guimberteau, M., Ducharne, A., Ciais, P., Boisier, J. P., Peng, S., Weirdt, M. D., & Verbeeck, H. (2014). Testing conceptual and physically based soil hydrology schemes against observations for the Amazon Basin. *Geoscientific Model Development*, *7*(3), 1115–1136. https://doi.org/10.5194/gmd-7-1115-2014

Gyssels, G., Poesen, J., Bochet, E., & Li, Y. (2016). Impact of plant roots on the resistance of soils to erosion by water: A review. *Progress in Physical Geography*, *29*, 189–217.

Harden, J. W., Sharpe, J. M., Parton, W. J., Ojima, D. S., Fries, T. L., Huntington, T. G., & Dabney, S. M. (1999). Dynamic replacement and loss of soil carbon on eroding cropland. *Global Biogeochemical Cycles*, *13*(4), 885–901. https://doi.org/10.1029/1999GB900061

Hastie, A., Lauerwald, R., Ciais, P., & Regnier, P. (2019). Aquatic carbon fluxes dampen the overall variation of net ecosystem productivity in the Amazon basin: An analysis of the interannual variability in the boundless carbon cycle. *Global Change Biology*, *25*(6), 2094–2111. https://doi.org/10.1111/gcb.14620

Heckmann, T., Cavalli, M., Cerdan, O., Foerster, S., Javaux, M., Lode, E., et al. (2018). Indices of sediment connectivity: Opportunities, challenges and limitations. *Earth-Science Reviews*, *187*, 77–108. https://doi.org/10.1016/j.earscirev.2018.08.004

Hoffmann, T., Schlummer, M., Notebaert, B., Verstraeten, G., & Korup, O. (2013). Carbon burial in soil sediments from Holocene agri-cultural erosion, Central Europe. *Global Biogeochemical Cycles*, *27*, 828–835. https://doi.org/10.1002/gbc.20071

Hurkmans, R. T. W. L., Terink, W., Uijlenhoet, R., Moors, E. J., Troch, P. A., & Verburg, P. H. (2009). Effects of land use changes on streamflow generation in the Rhine basin. *Water Resources Research*, *45*, W06405. https://doi.org/10.1029/2008WR007574

Isotta, F. A., Frei, C., Weilguni, V., Tadic, M. P., Lassegues, P., Rudolf, B., et al. (2013). The climate of daily precipitation in the Alps: Development and analysis of a high-resoluton grid dataset from pan-Alpine rain-gauge data. *International Journal of Climatology*, *34*, 1657–1675. https://doi.org/10.1002/joc.3794

Jobbagy, E. G., & Jackson, R. B. (2000). The vertical distribution of soil organic carbon and its relation to climate and vegetation. *Ecological Applications*, *10*(2), 423–436. https://doi.org/10.1890/1051-0761(2000)010[0423:TVDOSO]2.0.CO;2

Jones, R. J. A., Hiederer, R., Rusco, E., & Montanarella, L. (2005). Estimating organic carbon in the soils of Europe for policy support. *European Journal of Soil Science*, *56*(5), 655–671. https://doi.org/10.1111/j.1365-2389.2005.00728.x

Kinnell, P. I. A. (2005). Why the universal soil loss equation and the revised version of it do not predict event erosion well. *Hydrological Processes*, *19*(3), 851–854. https://doi.org/10.1002/hyp.5816

Kirkels, F. M. S. A., Cammeraat, L. H., & Kuhn, N. J. (2014). The fate of soil organic carbon upon erosion, transport and deposition in agricultural landscapes—A review of different concepts. *Geomorphology*, *226*, 94–105. https://doi.org/10.1016/j.geomorph.2014.07.023

Krinner, G., Viovy, N., de Noblet-Ducoudré, N., Ogée, J., Polcher, J., Friedlingstein, P., et al. (2005). A dynamic global vegetation model for studies of the coupled atmosphere-biosphere system. *Global Biogeochemical Cycles*, *19*, GB1015. https://doi.org/10.1029/2003GB002199

Kucharik, C. J., Foley, J. A., Delire, C., Fisher, V. A., Coe, M. T., Lenters, J. D., et al. (2000). Testing the performance of a dynamic global ecosystem model: Water balance, carbon balance, and vegetation structure. *Global Biogeochemical Cycles*, *14*(3), 795–825. https://doi.org/10.1029/1999GB001138

Lal, R. (2003). Soil erosion and the global carbon budget. *Environment International*, *29*(4), 437–450. https://doi.org/10.1016/S0160-4120(02)00192-7

Lal, R. (2010). Managing soils and ecosystems for mitigating anthropogenic carbon emissions and advancing global food security. *Bioscience*, *60*(9), 708–721. https://doi.org/10.1525/bio.2010.60.9.8

Larson, W. E., Pierce, F. J., & Dowdy, R. H. (1983). The threat of soil erosion to long-term crop production. *Science*, *219*(4584), 458–465. https://doi.org/10.1126/science.219.4584.458

Lauerwald, R., Regnier, P., Camino-Serrano, M., Guenet, B., Guimberteau, M., Ducharne, A., et al. (2017). ORCHILEAK: A new model branch to simulate carbon transfers along the terrestrial-aquatic continuum of the Amazon basin. *Geoscientific Model Development*, *10*, 3821–3859. https://doi.org/10.5194/gmd-10-3821-2017

Li, X., Niu, J., & Xie, B. (2014). The effect of leaf litter cover on surface runoff and soil erosion in northern China. *PLoS ONE*, *9*(9), e107789. https://doi.org/10.1371/journal.pone.0107789

Liu, S., Bliss, N., Sundquist, E., & Huntington, T. G. (2003). Modeling carbon dynamics in vegetation and soil under the impact of soil erosion and deposition. *Global Biogeochemical Cycles*, *17*(2), 1074. https://doi.org/10.1029/2002GB002010

Lugato, E., Paustian, K., Panagos, P., Jones, A., & Borrelli, P. (2016). Quantifying the erosion effect on current carbon budget of European agricultural soils at high spatial resolution. *Global Change Biology*, *22*(5), 1976–1984. https://doi.org/10.1111/gcb.13198

Melillo, J. M., Mcguire, A. D., Kicklighter, D. W., Moore, B., Vorosmarty, C. J., & Schloss, A. L. (1993). Global climate change and terrestrial net primary production. *Nature*, *363*(6426), 234–240. https://doi.org/10.1038/363234a0

Moore, D. I., & Burch, G. (1986). Physical basis of the length-slope factor in the universal soil loss equation. *Soil Science Society of America Journal*, *50*(5), 1294–1298. https://doi.org/10.2136/sssaj1986.03615995005000042x

Moore, D. I., & Wilson, P. J. (1992). Length-slope factors for the revised universal soil loss equation: Simplified method of estimation. *Journal of Soil and Water Conservation*, *47*, 423–428.

Morgan, R. P. C., Quinton, J. N., Smith, R. E., Govers, G., Poesen, J. W. A., Auerswald, K., et al. (1998). The European Soil Erosion Model (EUROSEM): A dynamic approach for predicting sediment transport from fields and small catchments. *Earth Surface Processes and Landforms*, *23*(6), 527–544. https://doi.org/10.1002/(SICI)1096-9837(199806)23:6<527::AID-ESP868>3.0.CO;2-5

Mualem, Y. (1976). A new model for predicting the hydraulic conductivity of unsaturated porous media. *Water Resources Research*, *12*(3), 513–522. https://doi.org/10.1029/WR012i003p00513

Muttil, N., & Jayawardena, A. W. (2008). Shuffled complex evolution model calibrating algorithm: Enhancing its robustness and efficiency. *Hydrological Processes*, *22*(23), 4628–4638. https://doi.org/10.1002/hyp.7082

Nadeu, E., Gobin, A., Fiener, P., van Wesemael, B., & van Oost, K. (2015). Modelling the impact of agricultural management on soil carbon stocks at the regional scale: The role of lateral fluxes. *Global Change Biology*, *21*(8), 3181–3192. https://doi.org/10.1111/gcb.12889

Naipal, V., Ciais, P., Wang, Y., Lauerwald, R., Guenet, B., & Van Oost, K. (2018). Global soil organic carbon removal by water erosion under climate change and land use change during AD 1850–2005. *Biogeosciences*, *15*(14), 4459–4480. https://doi.org/10.5194/bg-15-4459-2018

Naipal, V., Reick, C., Pongratz, J., & Van Oost, K. (2015). Improving the global applicability of the RUSLE model-adjustment of the topographical and rainfall erosivity factors. *Geoscientific Model Development*, *8*, 2893–2913. https://doi.org/10.5194/gmd-8-2893-2015

Naipal, V., Reick, C., Van Oost, K., Hoffmann, T., & Pongratz, J. (2016). Modeling long-term, large-scale sediment storage using a simple sediment budget approach. *Earth Surface Dynamics*, *4*(2), 407–423. https://doi.org/10.5194/esurf-4-407-2016

Nearing, M. A., Foster, G. R., Lane, L. J., & Finkner, S. C. (1989). A process-based soil erosion model for USDA-Water Erosion Prediction Project technology. *Transactions of ASAE*, *32*(5), 1587–1593. https://doi.org/10.13031/2013.31195

Neitsch, S. L., Arnold, J. G., Kiniry, J. R., & Williams, J. R. (2011). Soil and water assessment tool theoretical documentation Version 2009. Texas water resources institute technical report no. 406, College Station: Texas A&M University system.

Odongo, V. O., Onyando, J. O., Mutua, B. M., van Oel, P. R., & Becht, R. (2013). Sensitivity analysis and calibration of the Modified Universal Soil Loss Equation (MUSLE) for the upper Malewa catchment, Kenya. *International Journal of Sediment Research*, *28*(3), 368–383. https://doi.org/10.1016/S1001-6279(13)60047-5

Panagos, P., Borrelli, P., Meusburge, K., Alewell, C., Lugato, E., & Montanarella, L. (2015). Estimating the soil erosion cover-management factor at the European scale. *Land Use Policy*, *48*, 38–50. https://doi.org/10.1016/j.landusepol.2015.05.021

Panagos, P., Borrelli, P., Meusburge, K., van der Zanden, E., Poesen, J., & Alewell, C. (2015). Modelling the effect of support practices (P-factor) on the reduction of soil erosion by water at European scale. *Environmental Science & Policy*, *51*, 23–34. https://doi.org/10.1016/j.envsci.2015.03.012

Panagos, P., Borrelli, P., Poesen, J., Ballabio, C., Lugato, E., Meusburger, K., et al. (2015). The new assessment of soil loss by water erosion in Europe. *Environmental Science & Policy*, *54*, 438–447. https://doi.org/10.1016/j.envsci.2015.08.012

Panagos, P., Meusburger, K., Ballabio, C., Borrelli, P., & Alewell, C. (2014). Soil erodibility in Europe: A high-resolution dataset based on LUCAS. *Science of the Total Environment*, *479-480*, 189–200. https://doi.org/10.1016/j.scitotenv.2014.02.010

Parton, W. J., Schimel, D. S., Cole, C. V., & Ojima, D. S. (1987). Analysis of factors controlling soil organic matter levels in Great Plains grasslands. *Soil Science Society of America Journal*, *51*(5), 1173–1179. https://doi.org/10.2136/sssaj1987.03615995005100050015x

Pimentel, D. (2006). Soil erosion: A food and environmental threat. *Environment, Development and Sustainability*, *8*(1), 119–137. https://doi.org/10.1007/s10668-005-1262-8

Quine, T. A., & Zhang, Y. (2002). An investigation of spatial variation in soil erosion, soil properties, and crop production within an agricultural field in Devon, United Kingdom. *Journal of Soil and Water Conservation*, *57*, 55–65.

Regnier, P., Friedlingstein, P., Ciais, P., Mackenzie, F. T., Gruber, N., Janssens, I. A., et al. (2013). Anthropogenic perturbation of the carbon fluxes from land to ocean. *Nature Geoscience*, *6*, 597–607.

Regnier, P., Lauerwald, R., & Ciais, P. (2014). Carbon leakage through the terrestrial-aquatic interface: Implications for the anthropogenic CO_2 budget. *Procedia Earth and Planetary Science*, *10*, 319–324. https://doi.org/10.1016/j.proeps.2014.08.025

Renard, K. G., Foster, G. R., Weesies, G. A., Mccool, D. K., & Yoder, D. C. (1997). *Predicting soil erosion by water: A guide to conservation planning with the Revised Universal Soil Loss Equation (RUSLE)*. Washington, DC (USA): Agricultural Research Service.

Richards, L. A. (1931). Capillary conduction of liquids through porous mediums. *Physics*, *1*(5), 318–333. https://doi.org/10.1063/1.1745010

Rosenbloom, N. A., Doney, S. C., & Schimel, S. (2001). Geomorphic evolution of soil texture and organic matter in eroding landscapes. *Global Biogeochemical Cycles*, *15*, 365–381.

Rysman, J. F., & Lemaitre, Y. (2016). Spatial and temporal variability of rainfall in the Alps-Mediterranean Euroregion. *Journal of Applied Meteorology and Climatology*, *55*, 655–671. https://doi.org/10.1175/JAMC-D-15-0095.1

Sadeghi, S. H. R., Gholami, L., Darvishan, A. K., & Saeidi, P. (2014). A review of the application of the MUSLE model worldwide. *Hydrological Sciences Journal*, *59*, 365–375. https://doi.org/10.1080/02626667.2013.866239

Sadeghi, S. H. R., & Mizuyama, T. (2007). Applicability of the modified universal soil loss equation for prediction of sediment yield in Khanmirza watershed, Iran. *Hydrological Sciences Journal*, *52*(5), 1068–1075. https://doi.org/10.1623/hysj.52.5.1068

Schimel, D. S. (2010). Terrestrial ecosystems and the carbon cycle. *Global Change Biology*, *1*, 77–91.

Schönbrodt, S., Saumer, P., Behrens, T., Seeber, C., & Scholten, T. (2010). Assessing the USLE crop and management factor C for soil erosion modeling in a large mountainous watershed in Central China. *Journal of Earth Science*, *21*(6), 835–845. https://doi.org/10.1007/s12583-010-0135-8

Shangguan, W., Dai, Y., Duan, Q., Liu, B., & Yuan, H. (2014). A global soil data set for Earth system modeling. *Journal of Advances in Modeling Earth Systems*, *6*, 249–263. https://doi.org/10.1002/2013MS000293

Shi, Z. H., Cai, C. F., Ding, S. W., Wang, T. W., & Chow, T. L. (2004). Soil conservation planning at the small watershed level using RUSLE with GIS: A case study in the Three Gorge area of China. *Catena*, *55*(1), 33–48. https://doi.org/10.1016/S0341-8162(03)00088-2

Singh, R., Tiwari, K. N., & Mal, B. C. (2006). Hydrological studies for small watershed in India using the ANSWERS model. *Journal of Hydrology*, *318*(1-4), 184–199. https://doi.org/10.1016/j.jhydrol.2005.06.011

Sitch, S., Huntingford, C., Gedney, N., Levy, P. E., Lomas, M., Piao, S. L., et al. (2008). Evaluation of the terrestrial carbon cycle, future plant geography and climate-carbon cycle feedbacks using five dynamic global vegetation models (DGVMs). *Global Change Biology*, *14*(9), 2015–2039. https://doi.org/10.1111/j.1365-2486.2008.01626.x

Sitch, S., Smith, B., Prentice, I. C., Arneth, A., Bondeau, A., Cramer, W., et al. (2003). Evaluation of ecosystem dynamics, plant geography and terrestrial carbon cycling in the LPJ dynamic global vegetation model. *Global Change Biology*, *9*(2), 161–185. https://doi.org/10.1046/j.1365-2486.2003.00569.x

Smith, S. V., & Buddemeier, R. W. (2005). Fates of eroded soil organic carbon: Mississippi Basin case study. *Ecological Applications*, *15*(6), 1929–1940. https://doi.org/10.1890/05-0073

Smith, S. V., Renwick, W. H., Buddemeier, R. W., & Crossland, C. J. (2001). Budgets of soil erosion and deposition for sediments and sedimentary organic carbon across the conterminous United States. *Global Biogeochemical Cycles*, *15*(3), 697–707. https://doi.org/10.1029/2000GB001341

Stallard, R. F. (1998). Terrestrial sedimentation and the carbon cycle: Coupling weathering and erosion to carbon burial. *Global Biogeochemical Cycles*, *12*(2), 231–257. https://doi.org/10.1029/98GB00741

Tetzlaff, B., Friedrich, K., Vorderbrugge, T., Vereecken, H., & Wendland, F. (2013). Distributed modelling of mean annual soil erosion and sediment delivery rates to surface waters. *Catena*, *102*, 13–20. https://doi.org/10.1016/j.catena.2011.08.001

Tian, H., Yang, Q., Najjar, R. G., Ren, W., Friedrichs, M. A. M., Hopkinson, C. S., & Pan, S. (2015). Anthropogenic and climatic influences on carbon fluxes from eastern North America to the Atlantic Ocean: A process-based modeling study. *Journal of Geophysical Research: Biogeosciences*, *120*, 757–772. https://doi.org/10.1002/2014JG002760

Tifafi, M., Guenet, B., & Hatté, C. (2018). Large differences in global and regional total soil carbon stock estimates based on SoilGrids, HWSD, and NCSCD: Intercomparison and evaluation based on field data from USA, England, Wales, and France. *Global Biogeochemical Cycles*, *32*(1), 42–56. https://doi.org/10.1002/2017GB005678

Todd-Brown, K. E. O., Randerson, J. T., Hopkins, F., Arora, V., Hajima, T., Jones, C., et al. (2014). Changes in soil organic carbon storage predicted by Earth system models during the 21st century. *Biogeosciences*, *10*, 18,969–19,004. https://doi.org/10.5194/bg-11-2341-2014

Tramontana, G., Jung, M., Schwalm, C. R., Ichii, K., Campsvalls, G., Ráduly, B., et al. (2016). Predicting carbon dioxide and energy fluxes across global FLUXNET sites with regression algorithms. *Biogeosciences*, *13*, 4291–4313. https://doi.org/10.5194/bg-13-4291-2016

Van Dijk, P. M., & Kwaad, F. J. P. M. (1998). Modelling suspended sediment supply to the Rhine drainage network; a methodological study. In W. Summer, E. Klaghofer, W. Zhang (Eds.), *Modelling soil erosion, sediment transport and closely related hydrological processes* (pp. 165–176). Vienna: IAHS Publication.

Van Genuchten, M. T. (1980). A closed-form equation for predicting the hydraulic conductivity of unsaturated soils. *Soil Science Society of America Journal*, *44*(5), 892–898. https://doi.org/10.2136/sssaj1980.03615995004400050002x

Van Hemelryck, H., Govers, G., Van Oost, K., & Merckx, R. (2011). Evaluating the impact of soil redistribution on the in situ mineralization of soil organic carbon. *Earth Surface Processes and Landforms*, *36*(4), 427–438. https://doi.org/10.1002/esp.2055

Van Oost, K., Govers, G., Quine, T. A., Heckrath, G., Olesen, J. E., De Gryze, S., & Merckx, R. (2005). Landscape-scale modeling of carbon cycling under the impact of soil redistribution: The role of tillage erosion. *Global Biogeochemical Cycles*, *19*, GB4014. https://doi.org/10.1029/2005GB002471

Van Oost, K., Quine, T. A., Govers, G., De Gryze, S., Six, J., Harden, J. W., et al. (2007). The impact of agricultural soil erosion on the global carbon cycle. *Science*, *318*(5850), 626–629. https://doi.org/10.1126/science.1145724

Van Oost, K., Verstraeten, G., Doetterl, S., Notebaert, B., Wiaux, F., Broothaerts, N., & Six, J. (2012). Legacy of human-induced C erosion and burial on soil-atmosphere C exchange. *Proceedings of the National Academy of Sciences of the United States of America*, *109*, 19,492–19,497. https://doi.org/10.1073/pnas.1211162109

Van Rompaey, A. J. J., Govers, G., & Baudet, M. (2010). A strategy for controlling error of distributed environmental models by aggregation. *International Journal of Geographical Information Science*, *13*, 577–590.

Verheijen, F. G. A., Jones, R. J. A., Rickson, R. J., & Smith, C. J. (2009). Tolerable versus actual soil erosion rates in Europe. Tolerable versus actual soil erosion rates in Europe. *Earth-Science Reviews*, *94*(1-4), 23–38. https://doi.org/10.1016/j.earscirev.2009.02.003

Vigiak, O., Malago, A., Bouraoui, F., Vanmaercke, M., Obreja, F., Poesen, J., et al. (2017). Modelling sediment fluxes in the Danube River basin with SWAT. *Science of the Total Environment*, *599-600*, 992–1012. https://doi.org/10.1016/j.scitotenv.2017.04.236

Viovy, N. (1996). Interannuality and CO_2 sensitivity of the SECHIBA-BGC coupled SVAT-BGC model. *Physics and Chemistry of the Earth*, *21*(5-6), 489–497. https://doi.org/10.1016/S0079-1946(97)81147-0

Wang, X., Cammeraat, E. L., Romeijn, P., & Kalbitz, K. (2014). Soil organic carbon redistribution by water erosion—The role of CO_2 emissions for the carbon budget. *PLoS ONE*, *9*, e96299. https://doi.org/10.1371/journal.pone.0096299

Wang, Z., Govers, G., Steegen, A., Clymans, W., Van den Putte, A., Langhans, C., et al. (2010). Catchment-scale carbon redistribution and delivery by water erosion in an intensively cultivated area. *Geomorphology*, *124*(1–2), 65–74. https://doi.org/10.1016/j.geomorph.2010.08.010

Wang, Z., Hoffmann, T., Six, J., Kaplan, J. O., Govers, G., Doetterl, S., & Van Oost, K. (2017). Human-induced erosion has offset one-third of carbon emissions from land cover change. *Nature Climate Change*, *7*(5), 345–349. https://doi.org/10.1038/nclimate3263

Williams, J. R. (1975). Sediment-yield prediction with universal equation using runoff energy factor, present and prospective technology for predicting sediment yield and sources. ARS-S-40. Brooksville, FL: US Department of Agriculture. *Agricultural Research Service*, 244-252.

Williams, J. R. (1995). The EPIC model. In V. P. Singh (Ed.), *Computer models of watershed hydrology* (pp. 909–1000). Highlands Ranch: Water Resources Publications.

Wischmeier, W. H., & Smith, D. D. (1978). *Predicting rainfall erosion losses—A guide to conservation planning. U.S.* Washington, DC: Gov. Print Office.

Yang, Y. S., & Shi, D. M. (1994). *Study on soil erosion in the Three Gorge area of the Changjiang River*. Nanjing, China: Southeast Universoty Press. (in Chinese)

Zaehle, S., Friend, A. D., Friedlingstein, P., Dentener, F., Peylin, P., & Schulz, M. (2010). Carbon and nitrogen cycle dynamics in the O-CN land surface model: 2. Role of the nitrogen cycle in the historical terrestrial carbon balance.*Global Biogeochemical Cycles*, *24*, GB1006. https://doi.org/10.1029/2009GB003522

Zhang, H., Liu, S., Yuan, W., Dong, W., Ye, A., Xie, X., et al. (2014). Inclusion of soil carbon lateral movement alters terrestrial carbon budget in China. *Scientific Reports*, *4*, 7247. https://doi.org/10.1038/srep07247

Zhang, Y., Degroote, J., Wolter, C., & Sugumaran, R. (2009). Integration of modified universal soil loss equation (MUSLE) into a GIS framework to assess soil erosion risk. *Land Degradation & Development*, *20*(1), 84–91. https://doi.org/10.1002/ldr.893

Zhou, P., Luukkanen, O., Tokola, T., & Nieminen, J. (2008). Effect of vegetation cover on soil erosion in a mountainous watershed. *Catena*, *75*(3), 319–325. https://doi.org/10.1016/j.catena.2008.07.010

Zobler, L. (1999). *Global soil types, 1-degree grid (Zobler)*. Oak Ridge, Tennessee, USA: ORNL DAAC. https://doi.org/10.3334/ORNLDAAC/418